

**CHANNEL-TUNABLE MODE-LOCKED LASER  
TRANSMITTER FOR OTDM NETWORKS AND  
MODELING OF MODE-LOCKED SEMICONDUCTOR  
LASER**

BY  
HUNG Wai

A Thesis Submitted in Partial Fulfillment of the Requirements  
for the Degree of Master of Philosophy  
Division of Information Engineering  
©The Chinese University of Hong Kong  
July 2000

The Chinese University of Hong Kong holds the copyright of the thesis. Any person(s) intending to use a part or whole of the materials in the thesis in a proposed publication must seek copyright release from the Dean of the Graduate School.



# Acknowledgement

Foremost, I would like to express my warmest gratitude towards my research supervisor, Prof. Lian Kuan Chen, for his guidance and support in my research and studies. I was introduced to the field of Optical Communications in an undergraduate course given by him and I have learnt a lot from him ever since. His working attitude and research ethics has been inspirational to me.

I would also like to express my deepest appreciation to Prof. Frank Tong, Prof. Ricky Ho and Dr. Simon Chan for the directions and helps they gave to my research.

Moreover, I am very grateful to thank Prof. Hai-Feng Liu, who has now returned to Australia, for sharing his in-depth knowledge in mode-locked semiconductor lasers with me and providing me with some hardware essential to my experiments.

A special thanks is extended to Mr. Y. W. Lee and Mr. Alex W. H. Siu for their technical assistance. Their knowledge in electronics and metal work has been essential to my project.

Furthermore, I would like to thank Dr. Yokoyama and Shimizu T. in NEC Optoelectronics Lab. for providing the 10GHz Mode-locked laser diode.

In addition, I would like to thank my colleagues from the Lightwave Communications Laboratory, Mr. Eddie Kong, Mr. Brian Sun, Mr. Kit Chan, Mr. Arthur Cheung, Mr. Ivan Ng, Mr. Peter Kung, Mr. Wen Yong Gang, Mr. Yu Hai Tao and Mr. Wu Ji Song for their encouragement and making my stay enjoyable.

I would like to acknowledge the Information Engineering Department staff for their friendly help.

Most of all, I wish to thank my father, mother, brother and Ms. Lilian Wai for their support and encouragement. This thesis is dedicated to my parents.

## 概要

本篇論文分爲兩部分。在第一部分中，我們建議了一個在時分復用光網絡傳輸節點中調節信道的新方案。這個方案利用了混合鎖模半導體激光器作爲光脈衝源。信道的調節是通過調節驅動鎖模激光器的電信號的相位。電信號相位的調節可以通過一條由電開關控制的可調延遲線。這個方案已在實驗中證明了可行性。論文中報告了實驗的設置和實驗結果。我們還在實驗中測量了鎖模激光器調入新信道所需的時間。

論文的第二部分旨在通過數字模擬，對被動和混合鎖模激光器的性質和動態行爲作更好的了解。我們用了大信號時域模擬法對鎖模激光器進行模擬。這種模擬法是基於解電磁場在激光器中的耦合方程式。在模擬中，我們特別注意了一些對被動和混合鎖模激光器的操作範圍及光脈衝寬度的因素。另外，我們也對電驅動信號的相位改變時，鎖模激光器的動態行爲做了詳細的模擬。最後，模擬的範圍還包括了次諧鎖模過程中產生的幅度調制現象。

# Abstract

This thesis is divided into two parts. In the first part of the thesis, we propose a new channel tuning scheme for a channel tunable transmitter in a Optical TDMA network node. This scheme make use of hybrid mode-locked laser diode as the pulse source. Channel tuning is achieved by shifting the phase of the RF driving signal. This is accomplished through variable electrical delay line controlled by RF switches. The proposed scheme is demonstrated experimentally. To determine the channel tuning time, the channel tuning transient of the mode-locked laser is also investigated.

The second part of the thesis aims at providing a better understanding, through numerical simulation, on the characteristics and dynamic behavior of the class of mode-locked diode lasers used in the first part. Large-signal time domain modeling method is used to carry out the simulation. This method is based on solving time dependent coupled wave equations using central-difference method, which allows a more accurate solution to be found. Using this model, passive and hybrid mode-locking can be simulated. In particular, we pay attention to factors that affect the mode locking regimes and the pulse width of the laser. The dynamic behavior of the hybrid mode-locked laser during the phase

change of the RF driving signal is also studied. Finally, the amplitude modulation phenomenon of subharmonic mode-locked laser is simulated and studied using this model.

# Contents

<b>1</b>	<b>Introduction</b>	<b>1</b>
1.1	All Optical Multi-Access Network . . . . .	1
1.2	Multi-access Techniques . . . . .	2
1.2.1	Wavelength-Division Multi-access (WDMA) . . . . .	2
1.2.2	Subcarrier Multi-Access (SCMA) . . . . .	3
1.2.3	Time-Division Multi-Access(TDMA) . . . . .	3
1.3	Numerical Modelling of Semiconductor Mode-locked laser . . . . .	4
1.4	Objective of this Thesis . . . . .	5
<b>2</b>	<b>Optical TDMA networks</b>	<b>7</b>
2.1	Introduction . . . . .	7
2.2	OTDM . . . . .	8
2.3	Network Architecture . . . . .	9
2.3.1	Broadcast Networks . . . . .	9
2.3.2	Switch-based networks . . . . .	10
2.4	Key technologies for optical TDMA Network . . . . .	13
2.4.1	High Repetition Rate Short Pulse sources . . . . .	13
2.4.2	Multiplexer and de-multiplexers . . . . .	15

2.4.3	Optical Clock Recovery . . . . .	17
2.4.4	All optical logic gates . . . . .	18
2.5	Summary . . . . .	19
<b>3</b>	<b>A Channel-Tunable Mode-locked Laser Transmitter for OTDM</b>	
	<b>Networks</b>	<b>20</b>
3.1	Introduction . . . . .	20
3.2	Principle of Operation . . . . .	21
3.3	Experimental Demonstration . . . . .	23
3.4	The Channel Tuning Transient . . . . .	25
3.5	Experimental Investigation of channel-tuning transient . . . . .	28
3.6	Summary . . . . .	37
<b>4</b>	<b>Modeling of Mode-Locked Semiconductor Laser</b>	<b>38</b>
4.1	Introduction . . . . .	38
4.2	Principle of Mode-Locking . . . . .	39
4.3	Simulation Model . . . . .	41
4.3.1	Travelling Wave Rate Equation Analysis . . . . .	41
4.3.2	Large Signal Time Domain Mode-locked Laser Model . . . . .	42
4.3.3	Modeling of Spontaneous Noise . . . . .	44
4.3.4	Modeling of Self-phase Modulation . . . . .	44
4.3.5	Frequency Dependent Gain Profile . . . . .	45
4.3.6	Computation Procedure . . . . .	45
4.4	Device Parameters . . . . .	47
4.5	Simulation Results on Passive Mode-locking . . . . .	48
4.5.1	Pulse Repetition Rate under Passive Mode-locking . . . . .	48

4.5.2	The effect of Differential Gain and Differential Absorption on Mode-locking Regimes . . . . .	50
4.5.3	The Effects of Linewidth Enhancement Factor and Ab- sorber Carrier Lifetime on Mode-locking Pulse Width . .	53
4.6	Simulation Results on Hybrid and Subharmonic Mode-locking .	54
4.6.1	Modeling the Effect of Modulation on Absorber Section .	54
4.6.2	Modulation Phase Change Dynamics . . . . .	55
4.6.3	Subharmonic Mode-Locking Induced Amplitude Modulation	62
4.7	Summary . . . . .	64
<b>5</b>	<b>Conclusion</b>	<b>66</b>
5.1	Summary of the Thesis . . . . .	66
5.2	Future Work . . . . .	67
	<b>Bibliography</b>	<b>69</b>

# List of Figures

2.1	Bit interleaved TDM and packet interleaved TDM . . . . .	8
2.2	Network topologies for broadcast networks . . . . .	10
2.3	A generic packet switching network . . . . .	11
2.4	A routing node for packet switching network . . . . .	11
2.5	(a) Manhattan street network (b) shuffle network . . . . .	12
2.6	mode-locked fiber ring laser . . . . .	13
2.7	(a) NOLM (b) TOAD . . . . .	15
2.8	Ultrafast Nonlinear Interferometer . . . . .	17
3.1	The structure of an MLLD . . . . .	22
3.2	The principle of channel tuning . . . . .	23
3.3	schematic of a Channel tunable transmitter . . . . .	24
3.4	MLLD mounted on an LD carrier . . . . .	25
3.5	(a) Autocorrelation trace of the optical pulses generated by MLLD (b) Optical Spectrum of the mode-locked pulses . . . . .	26
3.6	RF spectrum of the optical output . . . . .	27
3.7	Schematic of the channel-tuning delay circuit . . . . .	28
3.8	10GHz optical pulse waveforms after being tuned to different channels (100ps/div) . . . . .	29

3.9	Experimental setup to investigate channel tuning transient . . .	30
3.10	The output of the Transient experiment . . . . .	31
3.11	Channel tuning transient experiments using (a) FP gain-switched laser (b) Mode-Locked fiber ring laser . . . . .	32
3.12	The output of the RF mixer . . . . .	33
3.13	Typical Channel Tuning waveform form FP Gain-switched laser	34
3.14	DC bias current vs Channel tuning time . . . . .	35
3.15	Ring laser output before and after undergoing a phase change in RF driving signal . . . . .	36
4.1	A typical mode locked pulse trains . . . . .	49
4.2	Different regimes of mode locking operation . . . . .	50
4.3	The output of mode-locked laser in CW, mode-locked and self- pulsation regimes . . . . .	51
4.4	Pulse width vs line width enhancement factor at different ab- sorber carrier lifetime . . . . .	53
4.5	Relative position of the pulses when the phase of the RF is changed for an amount of from 0 (a) to $\frac{7\pi}{4}$ (h) . . . . .	56
4.6	Transient time for laser output due to RF phase tuning . . . . .	57
4.7	The change of pulse width during phase tuning with 70% modu- lation of RF modulation . . . . .	58
4.8	The change of pulse width during phase tuning with 90% modu- lation of RF modulation . . . . .	59
4.9	The change of pulse amplitude during phase tuning with 70% modulation of RF modulation . . . . .	60

4.10	The change of pulse amplitude during phase tuning with 90% modulation of RF modulation . . . . .	61
4.11	Pulse train for subharmonic number 2, 3 4 and 5 respectively . .	63
4.12	Amplitude modulation parameter vs Subharmonic Number . . .	64

# Chapter 1

## Introduction

### 1.1 All Optical Multi-Access Network

Optical fibers are known to possess a huge capacity ( $> 30\text{THz}$  bandwidth). A large portion of these available capacities are, however, not utilized mainly due to the limited processing speed of the opto-electronic devices connected to the fiber. Therefore it is desirable to allow several communication nodes to share the same optical medium. To further increase the performance of the network, all-optical processing techniques can be employed at the network nodes so that O/E and E/O conversion can be avoided. As a result, all-optical multi-access network was evolved [1].

Contrast to optical long-haul transmission networks which simply transmit data from the source to the destination, multi-access networks further allow resource sharing among all network nodes and support channel add-drop. The key network functions in general include routing, multiplexing, demultiplexing and switching. In order to facilitate the multi-access, the transceiver at each

node should be channel-tunable and an efficient media access control (MAC) protocol is required to maximize the network throughput. Typical network elements include optical cross-connect (OXC), wavelength grating Router (WGR), tunable filters, tunable transmitters and receivers, channel multi/demultiplexers and optical add-drop multiplexers (OADM).

In the following section, three common kinds of optical multi-access networks, namely, wavelength division multi-access, time division multi-access (TDMA), and subcarrier multi-access (SCMA) will be briefly described.

## **1.2 Multi-access Techniques**

### **1.2.1 Wavelength-Division Multi-access (WDMA)**

In wavelength division multi-access networks (WDMA), each channel is represented by a specific wavelength. Wavelength division multiplexing (WDM) is used to combine all channels on the backbone. There are two types of WDMA networks, namely single-hop WDMA networks and multi-hop WDMA networks. In single-hop WDMA, the data stream does not have any opto-electronic conversion or wavelength conversion before it reaches its destination. They require wavelength-tunable devices such as wavelength-tunable filters and lasers, to set up the network connections. In multi-hop WDMA networks, there are some intermediate nodes to relay the data stream from the source to the destination and thus they do not require tunable transceivers. However, opto-electronic and electro-optic conversions may be needed at the intermediate nodes. In general both of single-hop and multi-hop WDMA networks are susceptible to the interchannel crosstalks, nonlinear effects, dispersion and optical amplifiers' ASE

noise.

### **1.2.2 Subcarrier Multi-Access (SCMA)**

In subcarrier multi-access networks (SCMA), single wavelength is used and each channel is represented by a specific RF subcarrier. Subcarrier multiplexing (SCM) is used to combine all channels on the backbone. The RF technology is quite mature and the RF components are economical and have good stability. However, the signal processing can only be done in electronic domain and the capacity is limited by various kinds of noises such as thermal noise, shot noise, relative intensity noise, intermodulation products, clipping and optical beat interference.

### **1.2.3 Time-Division Multi-Access(TDMA)**

In time division multi-access networks (TDMA) network, Optical Time Division Multiplexing technique is used to achieve channel multiplexing. There are two kinds of TDMA networks, namely bit-interleaved TDMA and packet-interleaved TDMA networks. In bit interleaved TDMA network, each channel occupies one time-slot (bit) in a TDM frame. They have a very stringent synchronization requirement and the time-slot (channel) tuning time should be of sub-nanosecond range when operate at high-speed (Gb/s). For packed-interleaved TDMA networks, the data packets from different nodes are transmitted in burst-mode and arrived asynchronously at the receivers. Therefore, some schemes should be used to avoid packet collision. Moreover, guard time should be added between adjacent packets and phase-locked loop are needed to extract the clock or phases in

each packet. Besides, there exists power variation from burst to burst due to different path attenuation between each node. Therefore, the receiver should have a large power dynamic range and the detection threshold should be adaptively changed to recover the data bits. Despite the stringent hardware requirements, TDMA network offers certain advantage over WDMA, such as higher aggregate bit rate on a single wavelength and simplified network management. More detail concerning TDMA, such as the network architecture and the required technologies to implemented optical TDMA networks will be discussed in next chapter.

### **1.3 Numerical Modelling of Semiconductor Mode-locked laser**

One of the key compoments for Optical Multi-Access network is optical short pulse source. Gain-switching, Q-switching and mode-locking are all possible methods to generate short pulses. The gain and Q switched lasers can generate optical pulses with pulse width of a few pico seconds and repetition rate in GHz range [2, 3]. With these techniques, the pulse width and frequency are restricted by gain dynamics and resonance frequency in the laser. The pulse repetition rate is limited to below 20GHz. Mode locking avoids these limitations and give repetition rates beyond 100GHz with nearly transform limited spectrums and low jitter. In recent years, passive and hybrid mode-locking have all been implemented using diode laser.

To better understand passive and hybrid diode lasers, a numerical model is needed to simulate their dynamic behavior. Classic mode-locked laser theory [4]

was applied to diode lasers by considering photon-electron coupling within the laser cavity. The locking of only 3 modes were considered. This provides little theoretical verification to experimental results in which several modes are usually locked. In recent years, large-signal time domain modelling method using time dependent coupled wave equations have been proposed to simulate laser devices [5]. With this method, an useful mode locking model can be constructed.

## **1.4 Objective of this Thesis**

The objective of this thesis is two-fold. The first part of the thesis aims at investigating the feasibility of using semiconductor mode-locked lasers as a channel tuning device in an optical TDMA network node. An overview of all-optical TDMA networks, the network architectures and key enabling technologies are first given in Chapter 2. Chapter 3 discusses the use of Mode-locked laser diode to construct a channel-tunable transmitter for Optical TDMA networks. The proposed scheme is demonstrated experimentally . The channel tuning transient is also investigated.

The second part of the thesis aims at providing a better understanding on the characteristics and dynamic behavior of the class of mode-locked diode lasers used in part 1. Chapter 4 describes a large-signal time domain modeling method to carry out numerical simulation on mode-locked laser diodes. A new set of equations are derive to solve the time-dependent coupling wave rate equation using central-difference method. Both passive and hybrid mode locking can be simulated using this model.

Finally, chapter 5 summarize this dissertation and suggests some directions

of research on both of the above topics.

# Chapter 2

## Optical TDMA networks

### 2.1 Introduction

High speed optical multi-access networks are being developed because of the ever-increasing demand for bandwidth in local, metropolitan and wide area networks. In recent years, WDM networks and systems with per channel data rate of 10 Gb/s are being deployed. By increasing the wavelength used within the network, the aggregate data rate can be increased considerably. As the channel density increases, however, the complexity of the WDM network also increases making the management of the network difficult. This has motivated the researchers to investigate another approach to increase the aggregate bit rate of the network, TDM. In TDMA networks, multiple time-domain channels can be interleaved to form a single data stream with channel rates exceeding 100 Gb/s [6]. The potential advantage of TDMA networks stem from the use of a single fast channel. Such a channel is simpler to manage and control. Variable quality of service (QoS) level can also be easily implemented [7] on this kind of channels.

## 2.2 OTDM

In OTDM network, optical signals representing data streams from multiple sources are interleaved in time to produce a single data stream. The interleaving can be done on a bit-by-bit basis as illustrated in Figure 2.1(a) or in the case where data are sent in packets, it can also be done on a packet-by-packet basis as shown in Figure 2.1(b). In both cases, guard time is needed to separate different frames. Another method to identify the boundary is to use framing pulses [8].

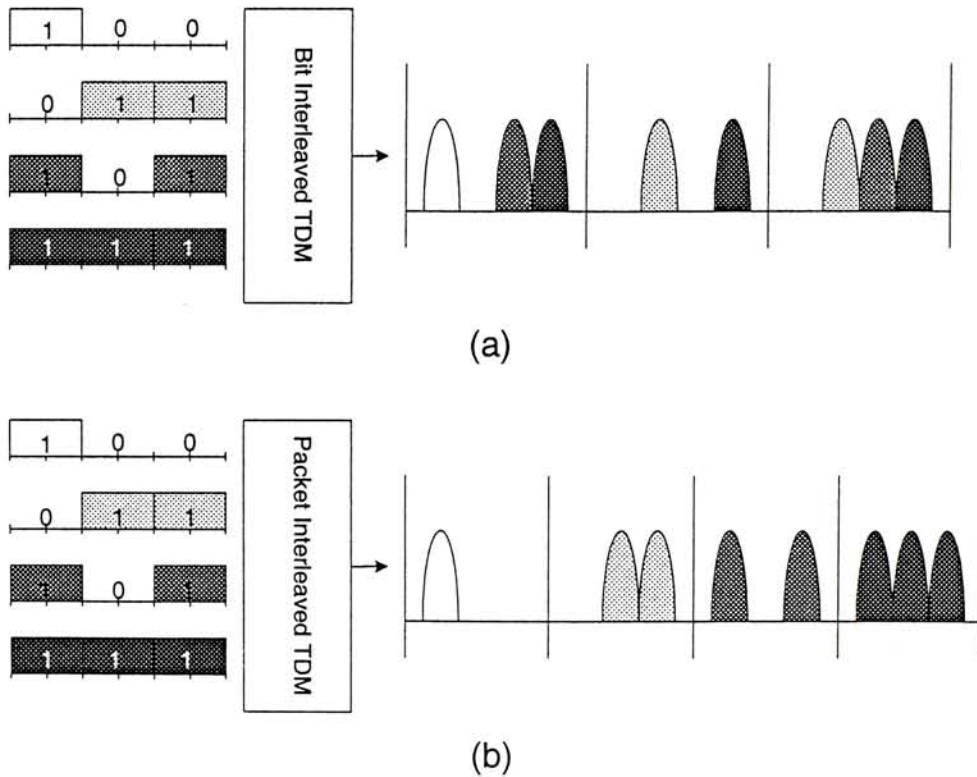


Figure 2.1: Bit interleaved TDM and packet interleaved TDM

## **2.3 Network Architecture**

### **2.3.1 Broadcast Networks**

Similar to WDM networks, an OTDM network can be either a broadcast network or a switch-based network. The topology of a broadcast network can either be a star or a bus/ring. In broadcast networks, there is no routing or switching within the network. All the network nodes are connected to a shared medium such as a passive star coupler or a single fiber bus or ring. Figure 2.2 illustrate some of the network topologies for broadcast network. To perform media access, each network node should be able to access one or more channels to send or receive data. This can be achieved through tuning transmitter or receiver to different time slots. Three types of node configurations are possible:

- fixed-tuned transmitter and tunable receiver (FTTR);
- tunable transmitter and fixed-tuned receiver (TTFR);
- tunable transmitter and tunable receiver (TTTR).

The last configuration provides the best flexibility but it requires costly tunable devices in both transmitter and receiver.

A multi-channel media-access protocol, such as ACTA [9], is required for this type of network so that network nodes can decide how to tune their transmitters and receivers.

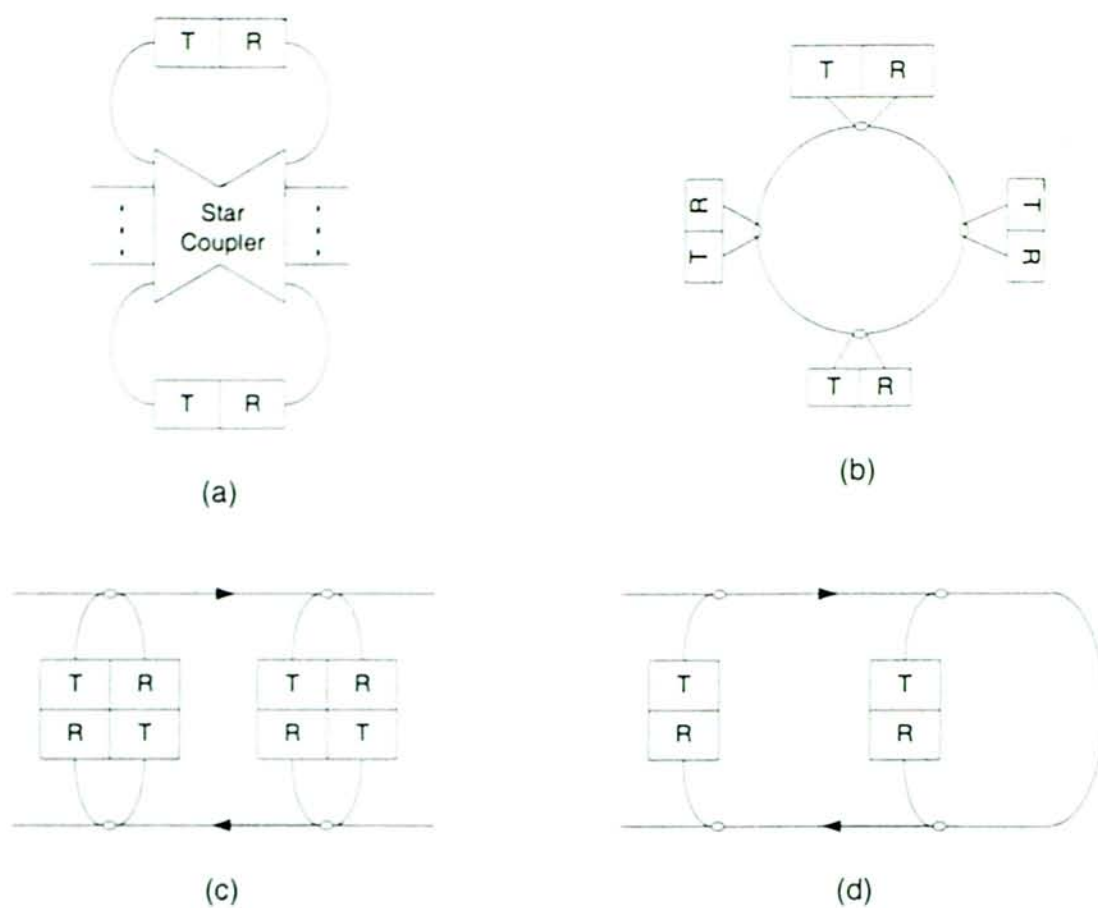


Figure 2.2: Network topologies for broadcast networks

### 2.3.2 Switch-based networks

Switch-based network, on the other hand, can have arbitrary mesh topology. Similar to the IP or ATM networks of today, switching and routing functionalities are incorporated into the network nodes. These functions are usually carried out in optical domain in order to provide packet switching service at a data rate that would be infeasible with electronic packet-switched networks.

A generic example of a packet switched network is shown in Figure 2.3. Packets sent by an end node usually traverse multiple links and hence multiple routing nodes before reaching their destinations. Therefore it is essential that

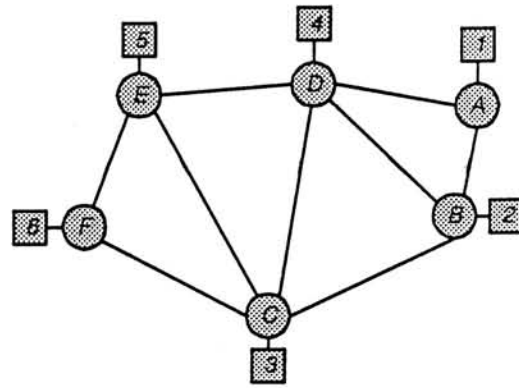


Figure 2.3: A generic packet switching network

the packets carry addressing information in their headers. A network node, upon receiving the packet, can then exam the packet header and decide the optimal route for the packet. A packet switching network node is shown in Figure 2.4. It carries out a number of tasks including (1) re-synchronization of incoming packets, (2) packet buffering, (3) packet header recognition and processing, (4) routing, flowing control and contention resolution.

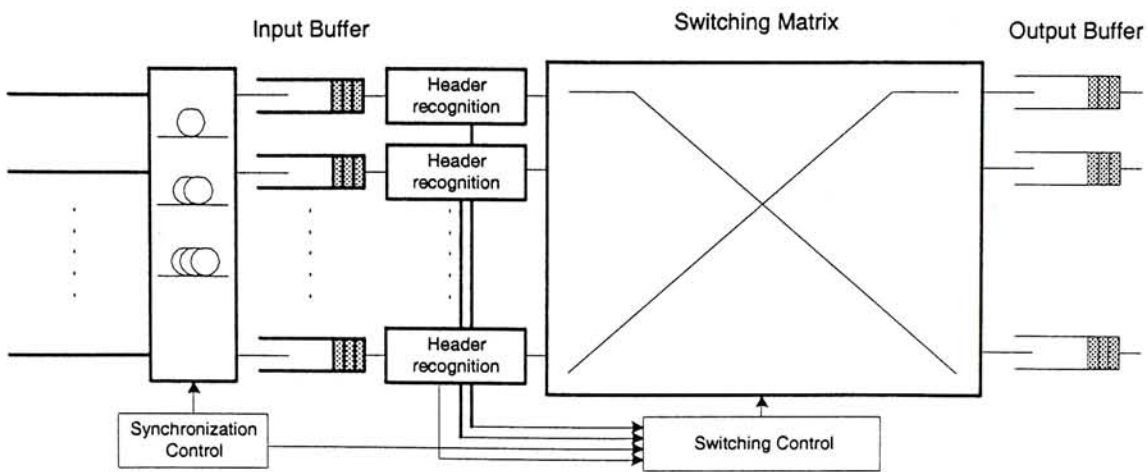


Figure 2.4: A routing node for packet switching network

There are tradeoffs between broadcast and switch based networks. The broadcast networks suffer from large splitting losses and are not scalable. Therefore, they are mainly suitable for LAN applications. The switch based networks are more scalable and suited for WAN applications. However, they are also significantly more complex since the network nodes have to perform many tasks optically. A working prototype of a full featured network node such as the one shown in Figure 2.4 has yet to be developed mainly due to the lack of practical optical components like ultrafast optical signal processor and random access memory. As a result, the choice of protocols (eg., deflection routing) and network topologies (eg., Manhattan street network [10] and shuffle network [11] as shown in Figure 2.5) for packet switching are limited.

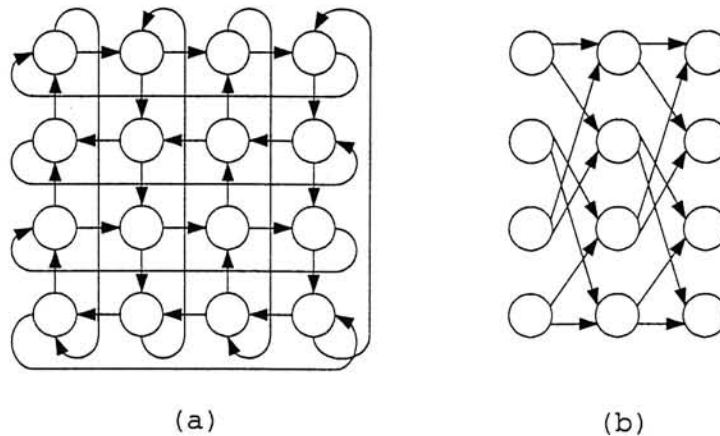


Figure 2.5: (a) Manhattan street network (b) shuffle network

## 2.4 Key technologies for optical TDMA Network

In this section, several key technologies for optical TDMA networks are briefly described.

### 2.4.1 High Repetition Rate Short Pulse sources

To increase channel capacity in OTDM networks, data bits are usually coded on return-to-zero (RZ) pulse trains. Thus laser sources that produce stable pulse trains with ultra-short pulses are critical to the successful operation of these optical networks. Furthermore, the generated pulses also need to be transform-limited to minimize pulse broadening due to dispersion and inter-symbol interference. Several options are available nowadays.

#### Active Mode-locked Fiber ring Laser

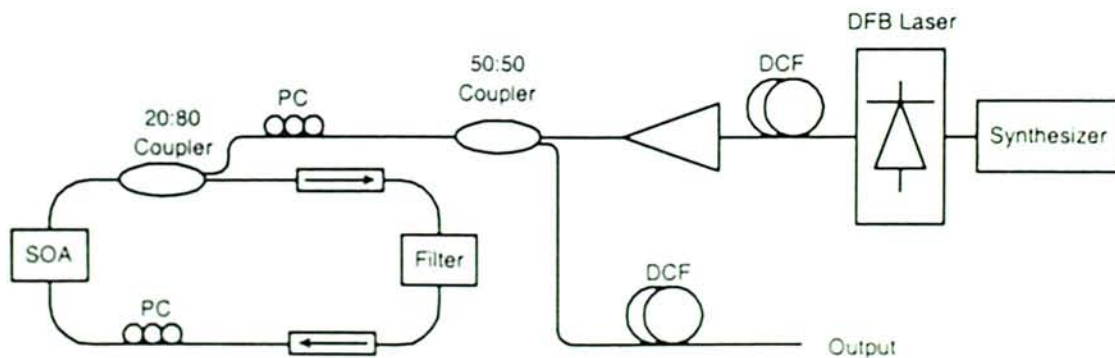


Figure 2.6: mode-locked fiber ring laser

Figure 2.6 shows the schematic of a mode-locked fiber ring laser with active

mode-locking. When the modulation frequency of the synthesizer matches the harmonics of the fundamental frequency of the cavity, optical pulses can be generated. 30-GHz optical pulse generation using this technique was reported in [12].

### **Semiconductor mode-locked laser**

Semiconductor mode-locked laser consists of [13] a gain section(s) and a saturable absorber(SA) section. They can be arranged in an (Colliding Pulse Mode-locking) CPM or (Self-Colliding Pulse Mode-locking) SCPM configuration. The repetition rate of these mode-locked lasers is closely related to the cavity length of the waveguide. If the length of the laser is  $L$ , the repetition rate of the pulses is  $v_g/2L$ , where  $v_g$  is the group velocity of the waveguide. These pulses can be synchronized to an external reference by either applying an RF signal to the SA section on top of the reverse bias voltage injecting an external optical pulse train. Transform limited pulses with pulse width less than 1ps can be generated using this method.

### **Gain Switched Lasers**

Gain switching [14] of laser diode is a simple way to generate short optical pulses. An RF signal can be applied directly to the gain section of a laser to produce optical pulses. A normal dispersion fiber can be used to achieve chirp compensation and the generated optical pulses can be further compressed to 5-7 ps pulse width with a repetition rate up to 20GHz.

## 2.4.2 Multiplexer and de-multiplexers

High speed channel multiplexing and demultiplexing are quite challenging in high-speed time division multiplexing. Here are some of the options.

### Channel Multiplexers

Low speed data stream have to be tuned to different time slots before combining them to form a higher speed data stream. Optical tunable delay lines are used to achieve this purpose. To reduce the insertion loss, external modulators can be integrated with In-P based waveguide arrays having different time delays to form a fast tunable delay line [15].

### Channel Demultiplexers

- *Nonlinear Optical loop mirrors (NOLM)*

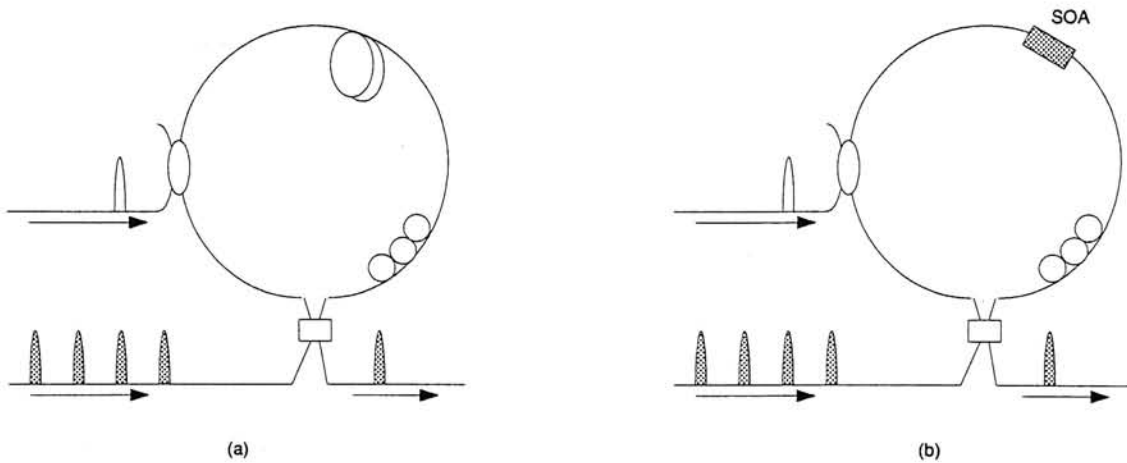


Figure 2.7: (a) NOLM (b) TOAD

Figure 2.7(a) shows a NOLM. It utilizes the interference between two counter-propagating signal streams with induced nonlinear phase shifts

within a fiber loop. A control pulse stream is injected into the loop to switch out the selected channel. 100 Gb/s to 6.3 Gb/s demultiplexing using NOLM was reported [16].

- *Terahertz Optical Asymmetric Demultiplexer (TOAD)*

The structure of TOAD [17] is similar to the NOLM, as shown in Figure 2.7(b) the basic difference is that the nonlinearities are introduced into the ring by a nonlinear element which may be a semiconductor device, for example, SOA. The most advantageous characteristics of this structure are its smaller required switching pulse power and the shorter ring length compared to NOLM.

- *Ultrafast Nonlinear Interferometer (UNI)*

The configuration of UNI was originally intended as a configuration for low repetition rate pump-probe experiment. It is shown in [18] that high speed switching (100 Gb/s) can also be achieved using this device. Figure 2.8 shows the configuration of a UNI. 40 Gb/s to 10 Gb/s demultiplexing using UNI was demonstrated.

- *Four-Wave Mixing (FMW)*

When a data signal and a strong pump signal, which are of different wavelengths, are injected simultaneously into a fiber or a semiconductor laser amplifier, a new wavelength, which contains the demultiplexed signal, can be generated by the nonlinear four-wave mixing effect. 400 Gb/s to 6.3 Gb/s demultiplexing using FWM was reported in [19].

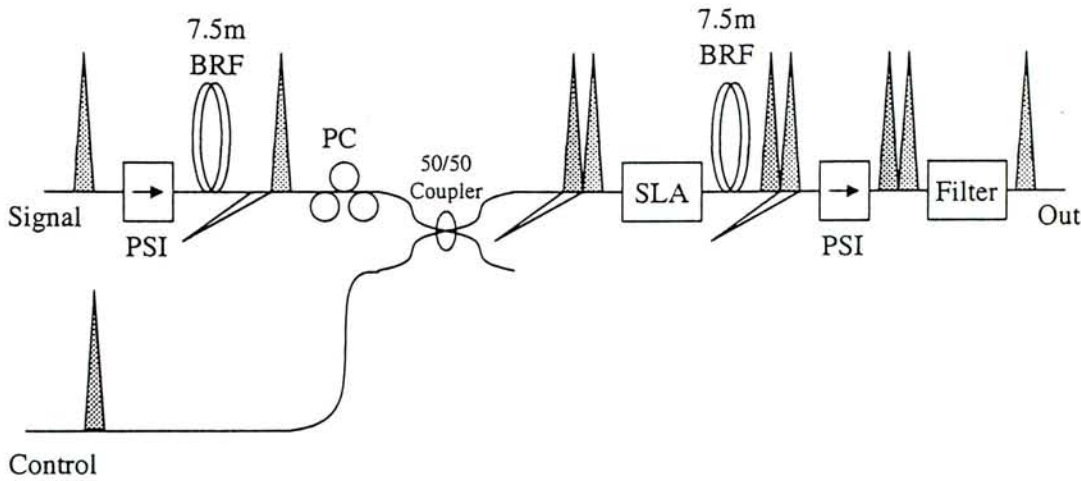


Figure 2.8: Ultrafast Nonlinear Interferometer

### 2.4.3 Optical Clock Recovery

All-Optical Clock Recovery circuit is a crucial part of an OTDM network as the receiver node needs to extract this timing reference from the incoming data stream before the received optical data can be detected, synchronized or regenerated correctly. Some of the approached are explained below:

#### Injection Locking

Injection locking utilizes a self-pulsation laser diode or a mode-locked laser whose output repetition frequency is locked to that of the injected optical pulse train. However, it may suffer from phase error in timing with respect to the injected signal when a lower speed clock is to be extracted. For semi-conductor mode-locked laser, this problem can be alleviated by cascading two mode-locked laser together with an SA optical gate [20]. 40-Gb/s clock extraction using mode-locked semi-conductor lasers has been demonstrated[20].

### **Phase lock loop circuit**

A travelling-wave laser diode amplifier is used as an all-optical phase detector yielding the phase difference (cross-correlated signal) between the input signal and the optical clock pulse train through all-optical gain modulation or FWM.

#### **2.4.4 All optical logic gates**

High speed OTDM network will operate at data rate as high as 100 Gb/s. It is important that digital data passing through a network node is processed optically at a high speed. To realize optical digital data processing, all optical logic gates become necessary. To date, most of the optical logic gates proposed take advantage of intensity-dependent transmission or the intensity-dependent refractive index of optical waveguides. Typically, short optical pulses are used to induce these nonlinearities because of their high peak power.

The simplest optical logic gates are NOT gates which can be implemented using cross gain saturation in active semiconductor waveguides. Another simple logic gate is all-optical AND gate based on four wave mixing. To realize logic gates other than AND and NOT, interferometric switches, based on intensity dependent refractive index effect of waveguides, can be used. The most frequently used interferometric switches are NOLM or TOAD. Using these switches, AND, NOT and XOR operations have been demonstrated. In addition, OR and NOR operations have been demonstrated using UNI [21].

Although all the key logic gates can be implemented optically nowadays, they suffer from a number of severe drawbacks. These optical logic devices are bulky in size, difficult to construct and hard to stabilize. Further, unlike electrical logic

devices, they usually need 3 optical inputs: 2 logic input and 1 clock stream. To induce the nonlinear effects in the interferometric switches effectively, the power requirement for these inputs are very high. Peak power of several dBm are necessary. These weaknesses limits the application of the above mentioned logic devices. For Optical TDMA networks to be deployed commercially, more compact and stable logic gates need to be developed.

## **2.5 Summary**

In this chapter, optical TDMA and the associated network architectures and key technologies are described in detail. Generally speaking, optical TDMA network offers the advantages of ultra high data rate, simpler network management and control (as only a single time domain channel is used) and provisions of flexible and true bandwidth-on-demand services and high speed digital signal processing for data regeneration, buffering and coding. It will become an important class of optical network that can satisfy the demand for broadband services in the future.

# Chapter 3

## A Channel-Tunable Mode-locked Laser Transmitter for OTDM Networks

### 3.1 Introduction

Recently, technologies for ultrahigh-speed optical time-division-multiplexed (OTDM) systems have advanced tremendously that terabit/s per channel capacity may be realized in the near future. Different from a point-to-point transmission system, for future broadband multimedia network using optical media, it is necessary to implement multi-access or switching functionality to allow interconnection between any two nodes.

In an bit-interleaved OTDMA networks, data intended for different nodes can be assigned to different channels (time slot) within one time frame. Therefore a channel-tunable transmitter or receiver that can tune its channel to a particular

time slot is required [22, 8]. Channel tuning time should be comparable to bit duration in order to reduce the guard time required between channel tuning, which is directly related to network throughput. Previously, channel tuning functionality was implemented using Optical Tunable Delay Line (OTDL) or fiber coupler connected to fibers with different lengths. The earlier configuration suffers from slow tuning time while the later one suffers from considerable insertion loss and thus degraded power budget.

Mode-locked lasers have been demonstrated to generate high repetition rate ultra-short optical pulses which are essential to high-speed OTDM applications [23]. In particular, semiconductor Mode-Locked Laser Diodes (MLLD), with their compact size, stable output and the ability to generate transform limited optical pulses with repetition rate as high as 40GHz, are considered a good source for OTDM networks. In this chapter, a scheme incorporating channel tuning ability into OTDM source using MLLD is proposed. A 10-Gb/s transmitter based on a hybrid MLLD capable of generating 2.6 ps optical pulses [24] is used in the experimental demonstration. Channel tuning is achieved by tuning the phase of the RF sinusoidal signal that drives the SA section of the MLLD. Section 3.2 will cover the operation principle of the channel tunable transmitter.

## **3.2 Principle of Operation**

A typical semiconductor MLLD consists of a laser cavity with a gain section, a modulation section, and a passive waveguide section. The gain section is for optical carriers generation and amplification, and the modulation section, which is usually a Saturable Absorber (SA), serves as a gate that allows optical signal

to pass through periodically.

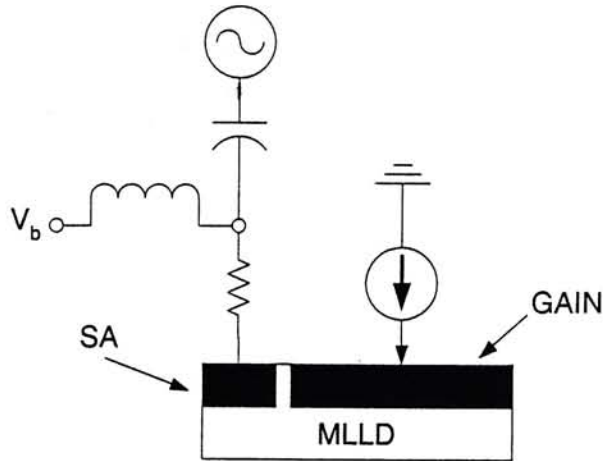


Figure 3.1: The structure of an MLLD

When a constant current is applied to the gain section and a reverse bias voltage is applied to the SA section, the device operates in passive mode-locking regime in which an impulse train with repetition rate equals the fundamental or harmonic of laser cavity round trip frequency is generated. The pulses generated, however, are not synchronized to any external signals and the time jitter of the pulses is large. This renders the pulses unusable for communication purposes. When An RF sinusoidal signal with a frequency ( $f_{mod}$ ) equal to one of the harmonics of laser cavity mode is applied to the SA, the steady impulse train will be synchronized to the phase of the driving RF signal. This mode of operation is called hybrid mode-locking. In this case, the MLLD can be used as the optical source for generating RZ pulses for OTDM networks.

Using this device, channel tuning functionality can also be realized. Since the pulses are synchronized with the input RF signal to the SA section, if the phase

of the driving signal is altered, optical pulses will also be shifted to different time slots after a transient period in which the original mode-locked pulses are suppressed and new pulses are formed.

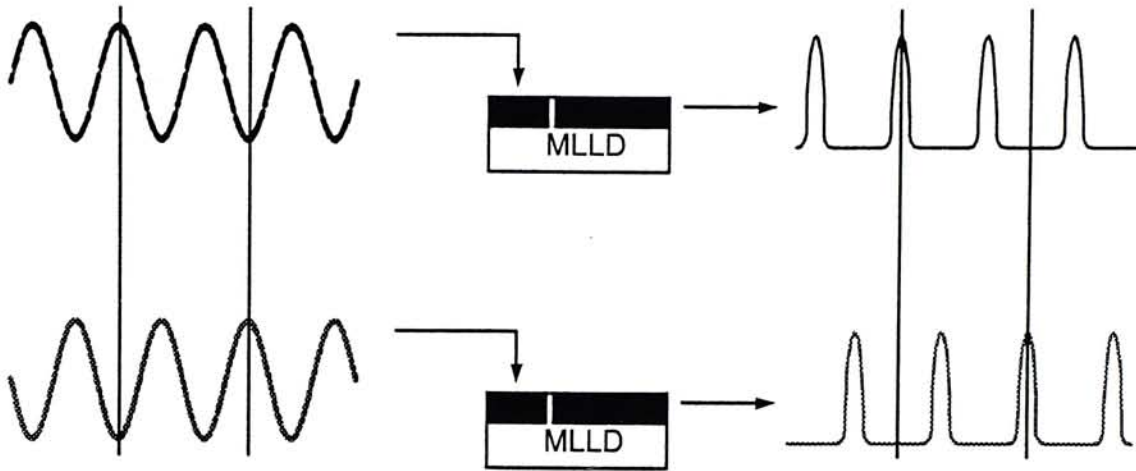


Figure 3.2: The principle of channel tuning

### 3.3 Experimental Demonstration

Figure 3.3 shows the schematic of a channel tunable transmitter using MLLD. An RF signal is delayed by an electrical channel-tunable delay circuit which has a switching time about 3 ns. After propagating through the delay line, the RF signal will have a different phase depending on the path it propagates. This RF signal is then used to drive the SA section of a mode-locked laser diode causing pulses in different time slot to be generated.

The MLLD device used in the experimental demonstration is shown in Figure 3.4. The length of the gain section is  $4344\mu m$  while the length of the SA section is  $150\mu m$ . This gives a round trip distance of  $8988\mu m$  thus the repetition rate

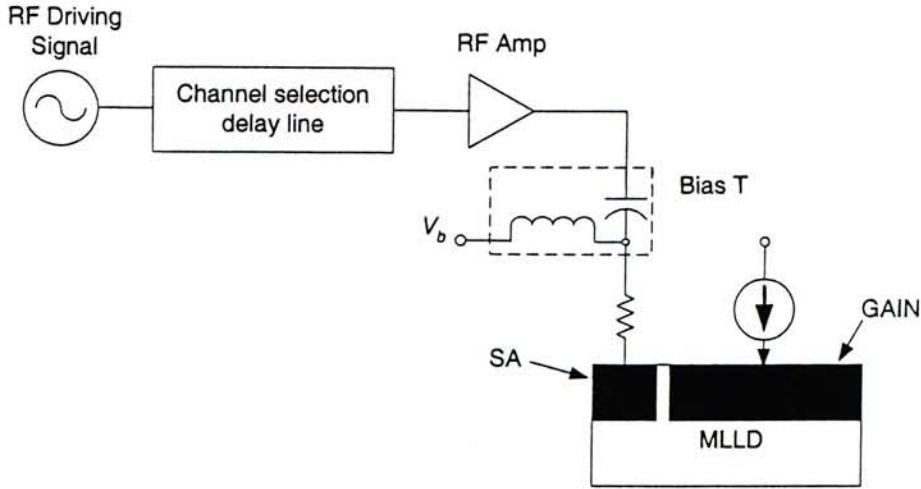


Figure 3.3: schematic of a Channel tunable transmitter

of the pulses is about 10GHz. The width of the pulse is found to be 2.6ps from autocorrelation measurements as shown in Figure 3.5(a). The optical spectrum is shown in Figure 3.5(b) and the RF spectrum in Figure 3.6.

The demonstration channel tuning circuit is designed for a 40-Gb/s and 4-channel optical TDM system. Each TDM frame has 4 time slots, each carrying a single bit and has a duration of  $\tau=25$ ps. The electronic channel tuning circuit consists of 2 stages of  $1 \times 2$  RF switches (HMC132C8 from Hitti microwave) as shown in Figure 3.7. These switches are controlled to select between the upper paths or the lower paths that have relative time delays of  $1\tau$  and  $2\tau$  respectively. Thus the RF signal can have a relative delay of  $0, \tau, 2\tau$  and  $3\tau$  respectively depending on the on-off status of the switches [22]. The delayed RF will then give rise to delayed mode-locked optical pulses. Figure 3.8 shows the waveform of the mode-locked pulses that are tuned to channel 1, 2, 3 and 4 respectively. Note that the pulse width appears to be considerably broader

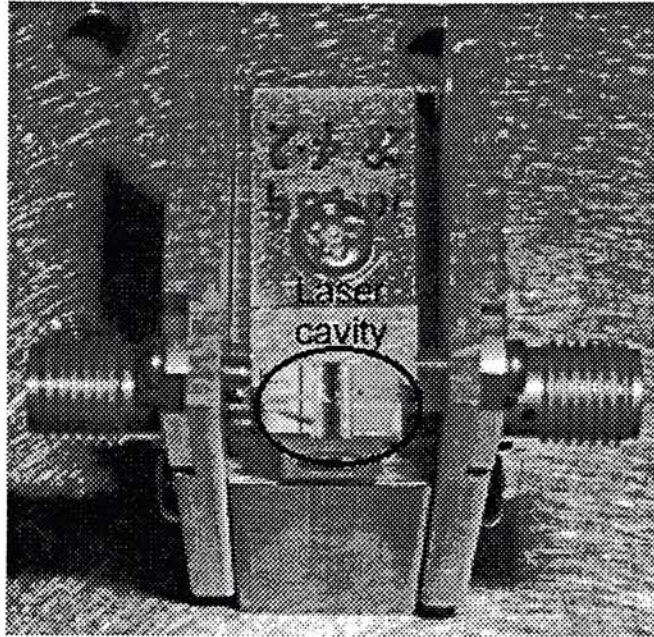


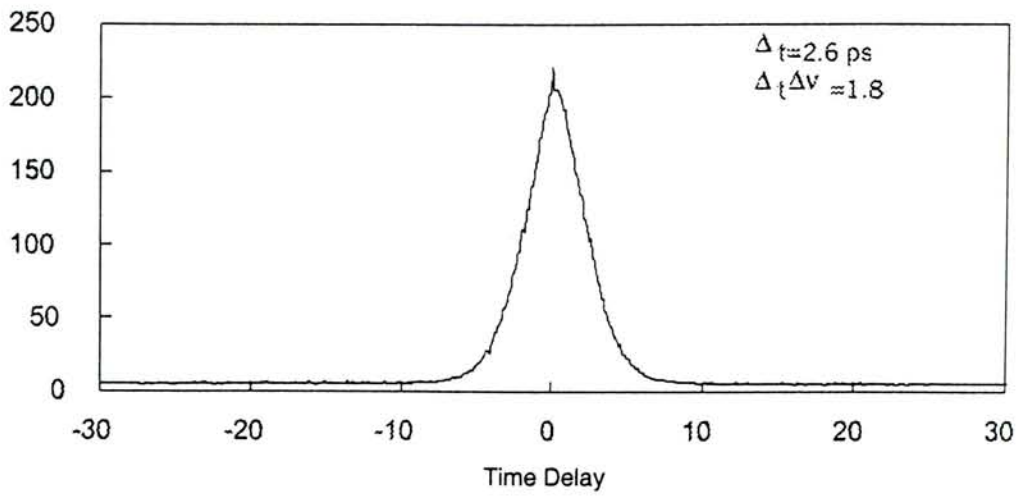
Figure 3.4: MLLD mounted on an LD carrier

owing to the fact that the signal was detected using a 20-Gb/s optical receiver.

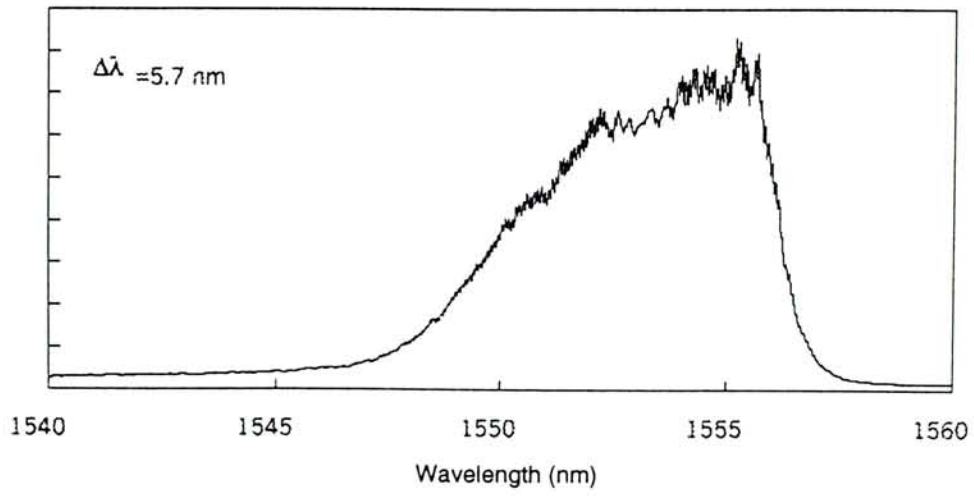
Though only 4 channels are implemented in the experiment, it demonstrates the feasibility of channel tuning scheme using Mode-locked lasers. A TDM system with more channels can be constructed with this MLLD. The number of channel is limited, in principle, by the ratio of the optical pulse separation and the optical pulse width. With this MLLD device, which generates optical pulses with 2.6ps pulse width at 10GHz, it is feasible to construct a TDM system with aggregate data rate of 100 Gb/s.

### **3.4 The Channel Tuning Transient**

One parameter that is of major concern to network designer is the duration of the transient period, which directly affects the channel-tuning time of the network's



(a)



(b)

Figure 3.5: (a) Autocorrelation trace of the optical pulses generated by MLLD  
(b) Optical Spectrum of the mode-locked pulses

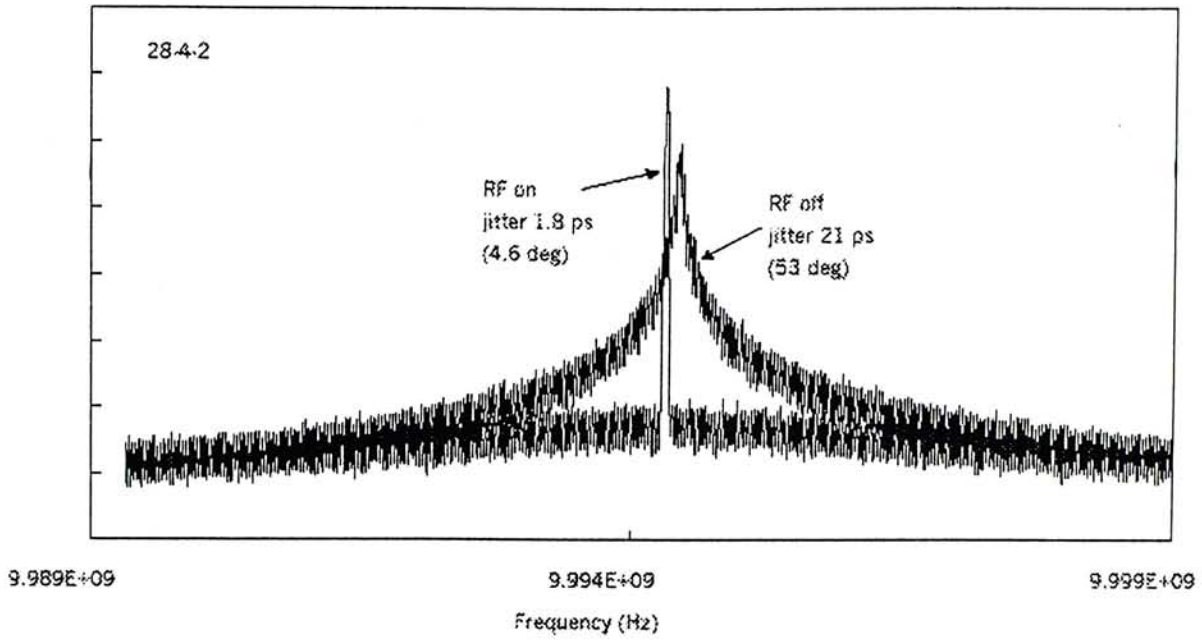


Figure 3.6: RF spectrum of the optical output

medium access control protocol. To achieve a high throughput network, it is necessary to minimize the channel tuning time.

Though the turn-on dynamic of a hybrid mode-locked lasers has previously been investigated [25], to our best knowledge, the transient effect due to the tuning of the RF driving signal has not been discussed. The behavior of the pulse generation during the channel-tuning transient is rather different from the turn-on transient which is the initial transient behavior exhibited by the laser without any prior driving signals. When the phase of the driving signal is tuned from one phase ( $\phi_1$ ) to the other ( $\phi_2$ ), the originally established mode-locked condition is destroyed and a new mode-locked condition will be re-established. Theoretically, channel-tuning transient depends on several factors, including the residual photon and electron carrier distribution in the laser cavity at the end of the first phase, the photon lifetime, the new phase of the driving signal and

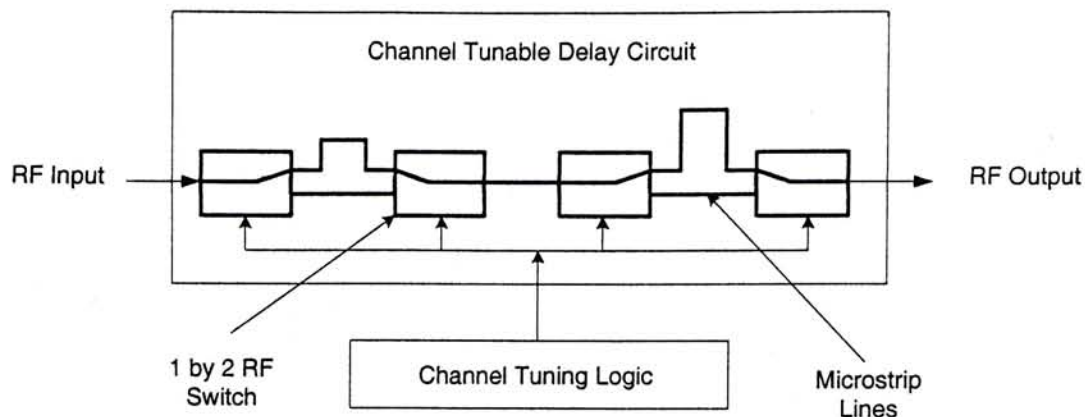


Figure 3.7: Schematic of the channel-tuning delay circuit

other factors as in the turn-on transient. It is expected if the phase change of the driving signal during channel tuning is small, it is easy to re-establish a new mode-locked condition.

### 3.5 Experimental Investigation of channel-tuning transient

The observation of the channel-tuning transient is not simple, especially at high repetition rate. To observe such a phenomenon, we switch the phase of the driving signal alternatively between two phases ( $\phi_1$  and  $\phi_2$ ). If the transient effect is periodic, we then can obtain the information of the channel-tuning characteristics of the mode-locked laser from a digital sampling oscilloscope.

The experimental setup for investigating the channel-tuning transient is illustrated in Figure 3.9. It consists of two stages. The first stage is responsible for generation of sinusoidal driving signals with periodic phase changes. The

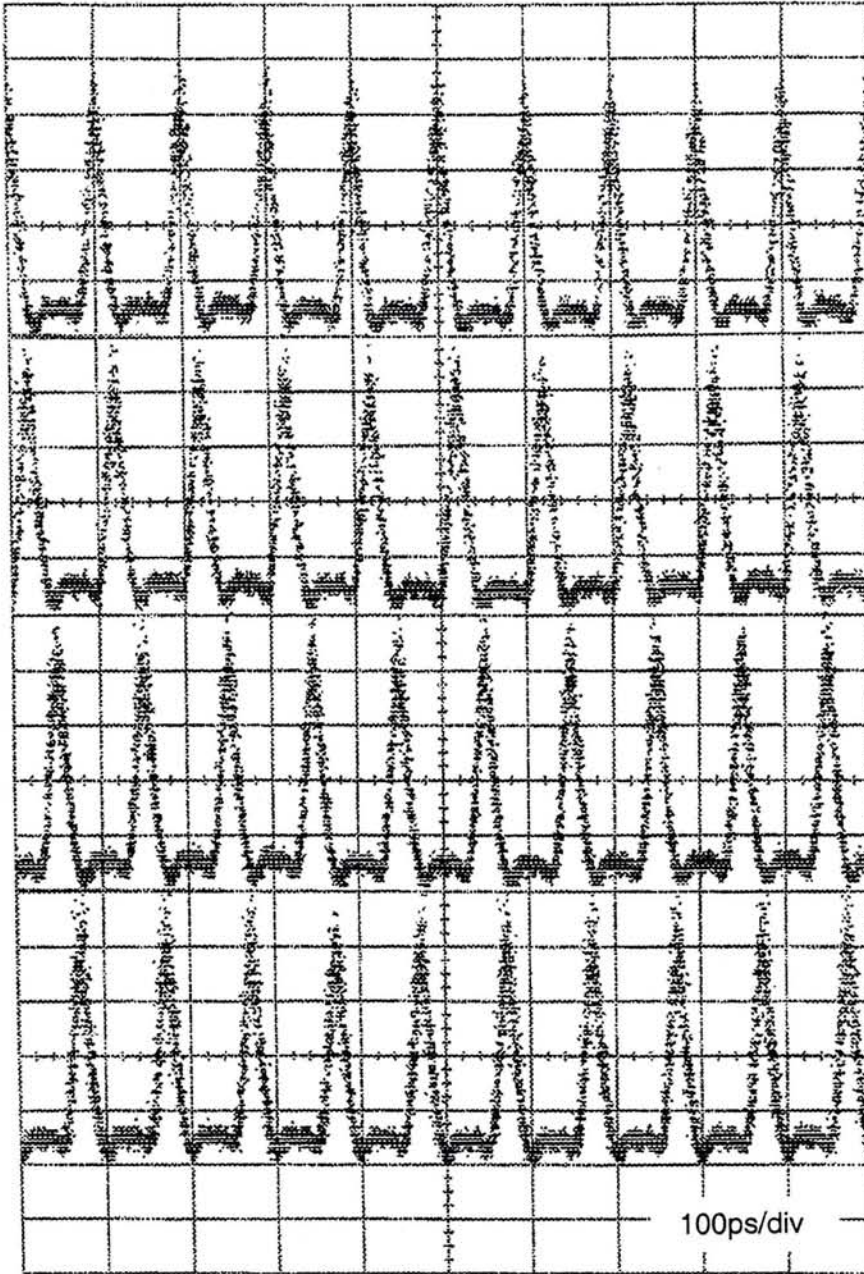


Figure 3.8: 10GHz optical pulse waveforms after being tuned to different channels (100ps/div)

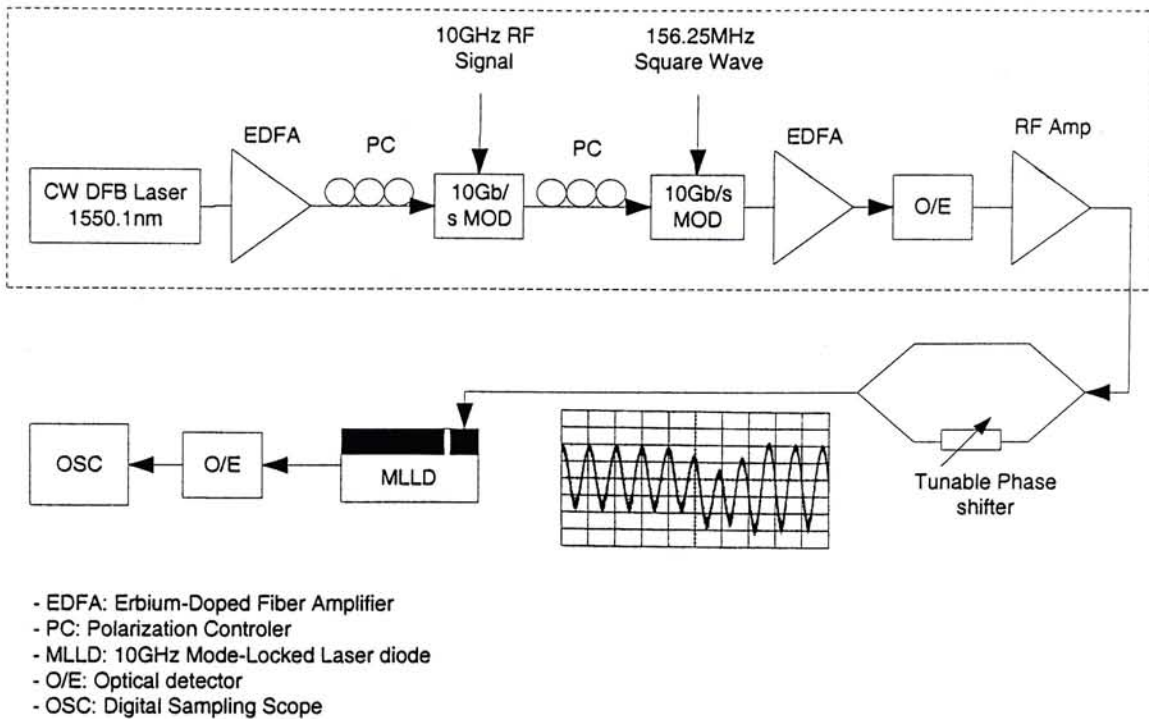


Figure 3.9: Experimental setup to investigate channel tuning transient

RF signals are then fed into the SA section of the MLLD. The generated RF signal is a 10-GHz sinusoidal signal that changes phase every 32 cycles. We use an optical means to minimize the switching time in phase change, thus reducing the effect of the transient time of electrical signal. A CW DFB laser emitting at 1550.10 nm is first amplified by an EDFA, and modulated externally at 10 GHz by a Mach-Zehnder external modulator. A second external modulator (IOC IOAP-MOD9001A) serves as an on-off modulator, gating the sinusoidal optical waveform into periodic on-off segments at 156.25 MHz. Both of the rise- and fall-time (20%-80%) of the IOC modulator are 30.8 ps, which are sufficiently short for switching on and off of the 10 GHz sinusoidal signal. The signals are optically amplified by a second EDFA to yield an average output power of 0.2

dBm. The optical signals are then received, amplified, and split into two different paths, one of which has a variable delay. The delay is carefully adjusted so that the on portion of one path coincides with the off portion of the other. The combined signal exhibits a periodic phase change every 3.2 ns, and the time it takes to change from one phase to another is about 200 ps as shown in the inset of Figure 3.9. The relative delay between the two phases is 20 ps. The resultant RF signals are used to drive the MLLD.

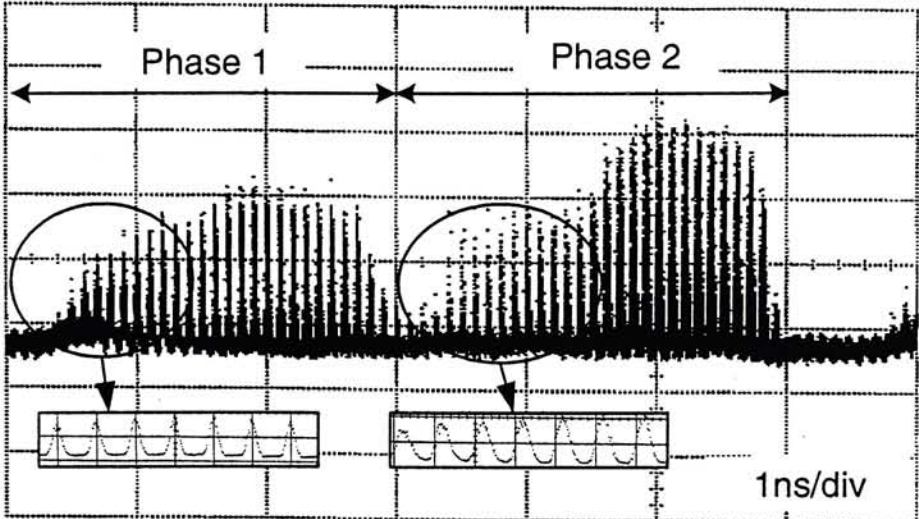


Figure 3.10: The output of the Transient experiment

Figure 3.10 shows the oscilloscope trace of the MLLD output. The transient is found to be  $< 2$  ns (20 pulses) for this device. At phase changes, it is observed that the amplitude of the pulse train gradually subsides and rebuilds again. The amplitude of the mode-locked pulses in one phase is higher than that in the other as the amplitude of the driving signals in the two phases are slightly different due to the unequal attenuation in the two delay paths. The details of the pulses generated are shown in the inset of Figure 3.10. The left trace is the optical

pulses generated in phase 1 and the right is for phase 2. The relative delay of the two traces is 20 ps (  $1/5$  of the bit period).

To compare this experimental result with other ultrafast pulse sources such as gain-switched FP laser and mode-locked fiber ring laser, which also require external RF driving signal, similar transient experiments have also been carried out with these devices. The experimental setup is shown in Figure 3.11. The

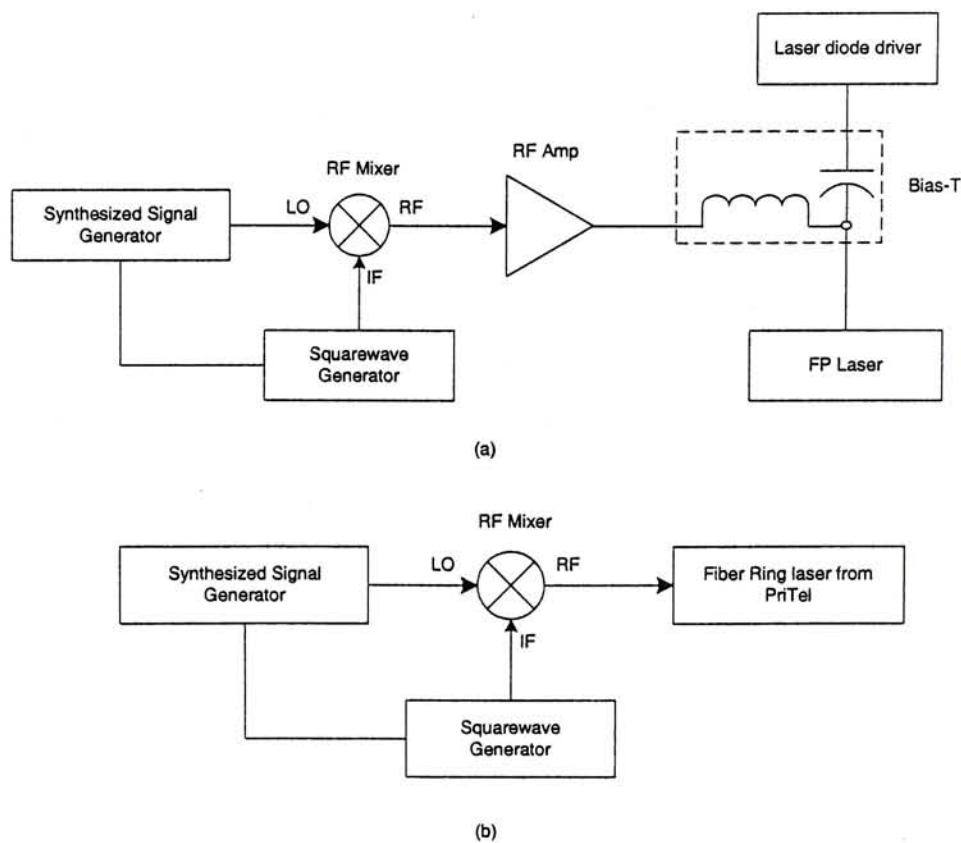


Figure 3.11: Channel tuning transient experiments using (a) FP gain-switched laser (b) Mode-Locked fiber ring laser

RF mixer, together with the signal generator and square wave generator, is capable of generating 10GHz RF signal with periodic  $\pi$  phase change within a very short duration, as shown in Figure 3.12 This signal is then used to gain

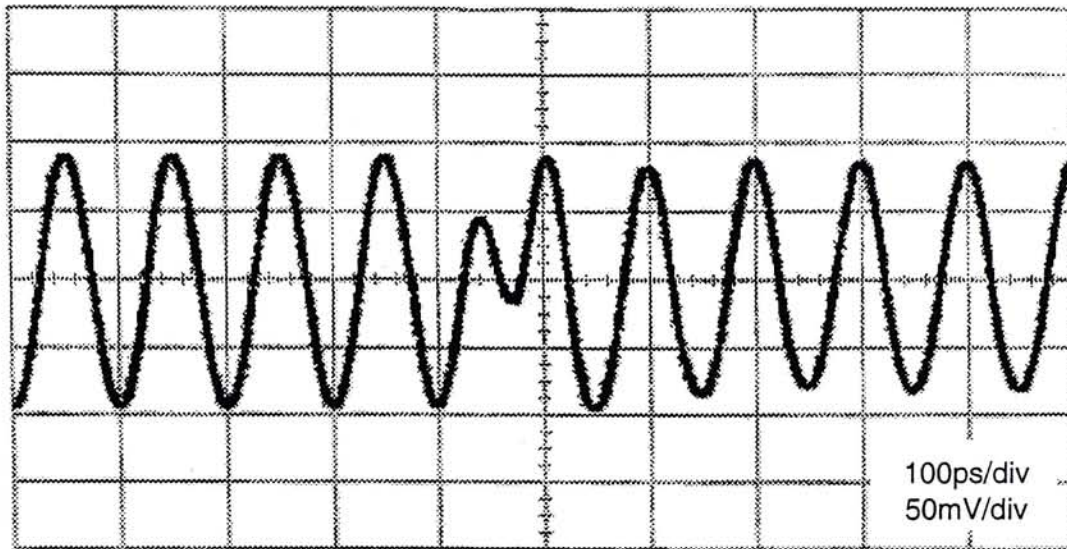


Figure 3.12: The output of the RF mixer

switch the FP laser or drive the fiber ring laser. In both cases, periodic changes in pulse position would occur after a transient period. For FP laser, the typical channel tuning waveform is shown in Figure 3.13. For a fixed repetition rate, the channel tuning time is found to depend on the DC bias current as well as the input RF power. The dependence of channel tuning time on these factors are shown in Figure 3.14. At a fixed DC bias, increasing RF modulation power would decrease the tuning time. If the RF power is fixed, increasing the DC bias will increase the channel tuning time as well. The maximum tuning time measured is 2.25 ns when the modulation power is 20.07dBm and DC bias is 50mA. Beyond that value, period-doubling will occur.

For fiber ring laser, the experiment was conducted on a ring laser clock source commercially available from PriTel, which has a fundamental frequency of 3.58MHz.

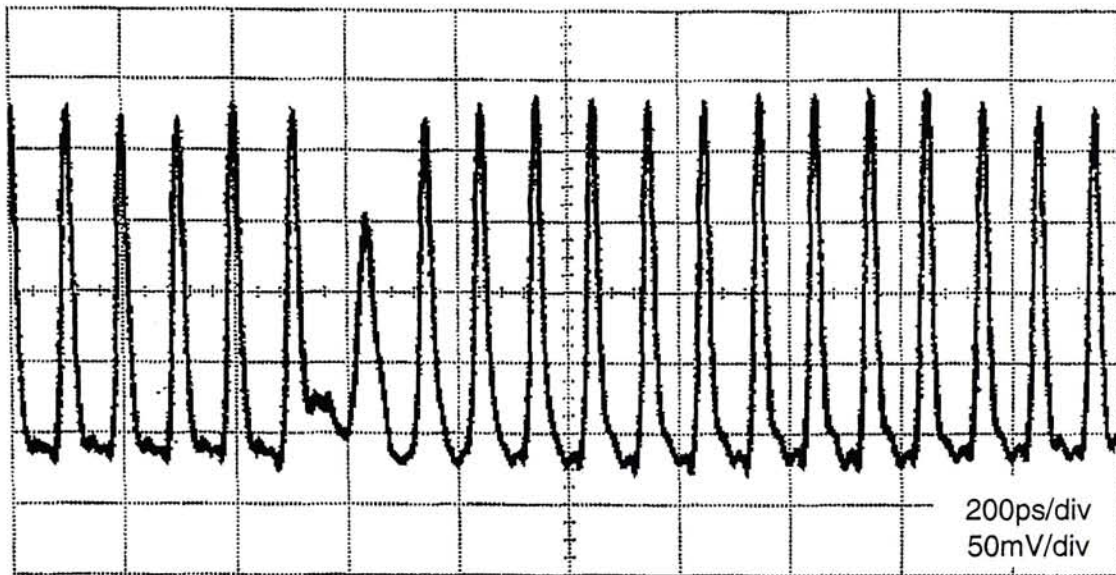


Figure 3.13: Typical Channel Tuning waveform from FP Gain-switched laser

Because the length of the fiber laser cavity is much longer than that of a mode-locked laser diode, the channel tuning transient occurs within a long period of time. The measured tuning time for this particular fiber ring laser is found to be 22 ns, nearly 10 times as long as that of a gain switched FP laser. This channel tuning time can be found by noticing that before phase switching, the optical pulses are located in the middle of the grid line as shown in the upper portion of Figure 3.15. After about 22 ns, the pulses become aligned to the grid lines of the sampling scope as shown in the lower portion of Figure 3.15.

Because the mode locked laser diode was accidentally damaged and the components necessary to carry out the experiment on FP and fiber ring laser did not arrive at our laboratory until a much later date, the same experimental setup cannot be used on the mode-locked laser. As the experimental setup on these 3 devices are different, the results cannot be compared directly. However, they do provide us with a rough comparison on the channel tuning time for these

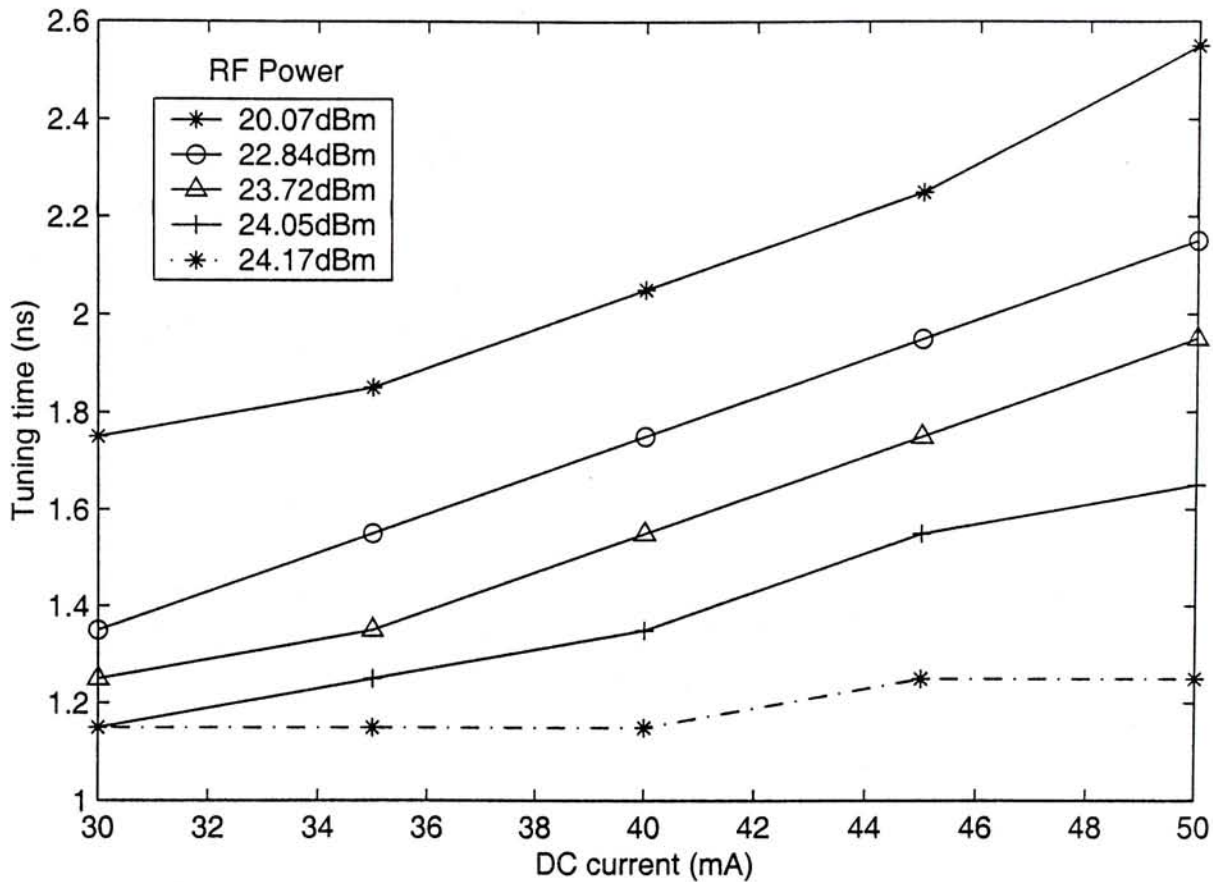


Figure 3.14: DC bias current vs Channel tuning time

devices.

In the following chapter, it is shown using numerical simulation that the channel tuning time for a mode-locked laser reaches its maximum if the amount of phase change is close to  $\frac{3\pi}{4}$ . In the mode-locked laser transient experiment described previously, the amount of phase change, however, is only  $\frac{2\pi}{5}$ . It is therefore reasonable to estimate that the maximum phase tuning time is more than 2ns if the device were to undergo a  $\pi$  phase change in the RF driving signal. Based on this assumption, we can then conclude that the phase tuning time for the gain switched FP laser is shorter than that of the mode-locked laser diode, which, in turn, is shorter than that of the fiber ring laser. Though

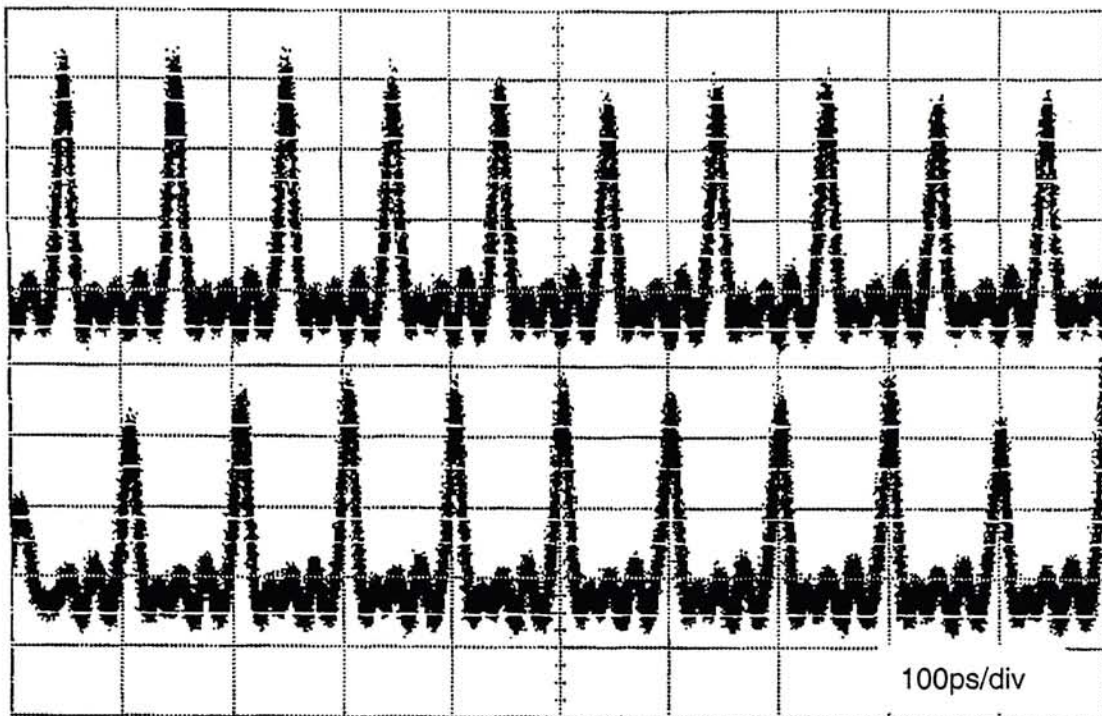


Figure 3.15: Ring laser output before and after undergoing a phase change in RF driving signal

the channel tuning time for the mode-locked laser is marginally longer than that of the FP laser, it remains a good pulse source for implementing channel tunable transmitter because of two reasons. The pulse width of mode locked pulses (2.6 ps) is generally shorter than that of gain-switched pulses (5-7 ps). Therefore, an extra pulse compression stage is usually needed to reduce the width of gain-switched pulses if they were to achieve the same pulse width as that of mode-locked pulses. Second, it is possible to use subharmonic mode-locking techniques to generate tunable mode-locked pulses using lower speed electronics whereas for gain-switched laser the driving RF signal must always match the repetition rate of the pulse.

## **3.6 Summary**

We demonstrated a 10-Gbit/s channel-tunable transmitter for OTDM networks operating at 40-Gbit/s aggregate data rate. Channel tuning is achieved by tuning the phase of the driving RF signal to a hybrid mode-locked laser. The corresponding transient is found to be 2 ns (20 pulses) which is longer than that of a gain switched FP laser.

# Chapter 4

## Modeling of Mode-Locked Semiconductor Laser

### 4.1 Introduction

Since its first demonstration [26], the research in picosecond or subpicosecond optical pulses generation using Mode-locked semiconductor lasers has had a lot of progresses. Passive mode-locked semiconductor lasers, in particular, have become promising candidates for high-speed applications because of their capability of producing ultra short high repetition rate optical pulses without the limitations imposed by driving electronics [27]. More importantly, it was shown theoretically that there is no fundamental limitation in mode-locking at frequencies below 100GHz [28]. With the recently developed Hybrid Mode-locking and Subharmonic Hybrid Mode-locking techniques, Mode-locked semiconductor lasers can now be able to provide stable pulse trains with very low level of phase noise and timing jitter. Therefore, mode-locked semiconductor lasers gives the

greatest potential for the development of reliable sources for ultra high-speed optical communications system.

In order to fully utilize the potentials of mode-locked semiconductor lasers, it is important to understand the behavior of these devices. Numerical simulation is one method to achieve this target.

In this chapter, the operation of hybrid and subharmonic hybrid mode locking in a semiconductor is simulated using a numerical model. The aims of the simulation are

- to investigate the range of laser material parameters leading to stable mode-lock pulses;
- to investigate the degree of amplitude modulation in subharmonic hybrid mode locking; and
- to investigate the phase tuning transient of a MLLD when the phase of the driving RF signal is switched from one value to another.

In the first section, the principle of mode-locking is introduced. Then, the numerical modelling method is described. Finally, the simulation result is presented.

## **4.2 Principle of Mode-Locking**

The generation of mode locked ultra short pulses is based upon the confinement of the energy in a laser cavity into a small spatial region or the concentration of the optical power normally divided between the whole set of fluctuations into just one. The laser emission often consists of a set of resonator mode  $\omega_m$ ,  $m=1$ ,

2, 3..., separated by  $\delta\omega$  [13]. The number of modes that oscillate is limited by the spectral bandwidth  $\delta\omega_g$  over which the laser gain exceeds the cavity loss. The output consists of a sum of frequency components that correspond to the oscillating modes, and the electric fields is given as (without taking into account the spatial distribution)[13]

$$E(t) = \sum_m A_m \exp i[(\omega_0 + m\delta\omega)t + \phi_m] \quad (4.1)$$

where  $A_m$  and  $\phi_m$  represent the amplitude and phase of the  $m$ th mode. In general, relative phases between the modes are randomly fluctuating. If nothing fixes the phases  $\phi_m$ , the laser output will vary randomly in time, the average power being approximately equal to the average of the individual modes. On the other hand, if the modes are forced to maintain a fixed phase and amplitude relationship, the output of the laser will be a periodic function of time:

$$E(t) = A_0 \frac{\sin[(k+1)\delta\omega t_1/2]}{\sin(\delta\omega t_1/2)} \exp(i\omega_0 t) \quad (4.2)$$

where  $k$  is the number of locked modes and  $t_1 = t + \delta\phi/\delta\omega$ .

In practice, mode-locking in semiconductor laser can be realized using a number of techniques, including active, passive, and hybrid methods.

1. active mode locking - when an external RF signal is used for gain/loss modulation of a single contact diode laser;
2. passive mode locking - when no external signal is used in a laser with a saturable absorber;
3. hybrid mode locking - when an external RF signal is used for gain/loss modulation in a multiple-contact diode laser or in a laser with an intra-cavity element that exhibits saturable absorption.

## 4.3 Simulation Model

### 4.3.1 Travelling Wave Rate Equation Analysis

The behavior of semiconductor laser can be described by rate equations for electron and photon density in the active layer of the device [29]. The two most important rate equations are the electron density rate equation and the photon density rate equation.

$$\frac{dP}{dt} = \beta R_{sp} + v_g GP - \frac{P}{\tau_P} \quad (4.3)$$

$$\frac{dN}{dt} = \frac{J}{qd} - R_{sp} - v_g GP \quad (4.4)$$

where  $P$  is the optical power,  $\beta$  is the spontaneous emission coupling factor,  $R_{sp}$  is the rate of recombination of excess carriers,  $v_g$  is the group velocity,  $G$  represents the gain per unit length for stimulated emission,  $\tau_P$  is the photon carrier lifetime,  $N$  is the carrier concentration,  $J$  is the current density,  $q$  is the electron charge and  $d$  represents the thickness of the active region.

Although the rate equation may be used to study both the transient and steady state behavior of the semiconductor laser, their merits are only limited to lumped interaction where the device is considered as a whole. This theoretical model cannot give explicit information about the frequency of oscillation, even if one uses specific information about gain as a function of frequency. Furthermore, the rate equations neither make allowance for nonuniformities in the field nor can they allow for the optical fields's phase which is important for mode-locked lasers [30]. For these reasons, a travelling wave field analysis approach is essential

for successful simulation of mode-locking.

The fundamental of travelling wave field analysis is a set of coupled travelling wave equations describing the propagation of optical field in a waveguide. This set of equations were originally developed for DFB laser [5].

The electrical field in the waveguide of a laser diode can be written as

$$E(z, t) = [E^+(z, t)e^{-i\beta_0 z} + E^-(z, t)e^{i\beta_0 z}]e^{-i\omega_0 t} \quad (4.5)$$

where  $\omega_0$  is the reference frequency and  $\beta_0$  is the propagation constant at Bragg frequency.  $E^+(z, t)$  and  $E^-(z, t)$  represent the forward and reverse waves in the waveguide, respectively.  $\omega_0$  is normally selected at the frequency of the gain peak. Inside a laser cavity, the fields  $E^+(z, t)$  and  $E^-(z, t)$  satisfy the time-dependent coupled wave equations, expressed as

$$\left(\frac{1}{v_g} \frac{\partial}{\partial t} + \frac{\partial}{\partial z}\right)E^+(z, t) = (g - i\delta - \alpha_s - h_l)E^+(z, t) + i(\kappa + ih_l)E_-(z, t) + s_+ \quad (4.6)$$

$$\left(\frac{1}{v_g} \frac{\partial}{\partial t} + \frac{\partial}{\partial z}\right)E^-(z, t) = (g - i\delta - \alpha_s - h_l)E^-(z, t) + i(\kappa + ih_l)E_+(z, t) + s_- \quad (4.7)$$

$E^+(z, t)$  and  $E^-(z, t)$  are forward and backward propagating E fields respectively.  $\kappa$  is the coupling coefficient between forward and backward waves.  $v_g$  is the group velocity,  $\delta$  is the detuning factor.  $h_l$  determines the radiation loss for the second order grating and  $\alpha_s$  is the waveguide loss caused by free electron absorption and scattering. The spontaneous noise coupled into the forward and backward fields are given as  $s_+$  and  $s_-$ .

### 4.3.2 Large Signal Time Domain Mode-locked Laser Model

In this section, the fundamentals of the Large-Signal time domain model is presented for calculating the dynamic response of a mode-locked Fabry-Perot

Semiconductor Laser. The algorithm is based on solving the time-dependent coupled wave equations.

Fabry-Perot Semiconductor mode-locked Laser consists of gain sections and an absorber section. Unlike a DFB laser, grating structures are absent from the active gain area, thus no coupling occurs between the forward and backward fields. The fields  $E^+(z, t)$  and  $E^-(z, t)$  time-dependent coupled wave equations inside the laser cavity can then be simplified to

$$\frac{1}{v_g} \frac{\partial E^+(z, t)}{\partial t} + \frac{\partial E^+(z, t)}{\partial z} = (g - i\delta - \alpha_s)E^+(z, t) + s_+ \quad (4.8)$$

$$\frac{1}{v_g} \frac{\partial E^-(z, t)}{\partial t} + \frac{\partial E^-(z, t)}{\partial z} = (g - i\delta - \alpha_s)E^-(z, t) + s_- \quad (4.9)$$

The complex fields  $E^\pm(z, t)$  include the amplitude and phase information. The spontaneous noise is driven by  $s_+$  and  $s_-$  which couple into the forward and backward fields.  $v_g$  is the group velocity.  $\alpha_s$  is the waveguide loss caused by free electron absorption and scattering.

The field gain  $g$  is given by

$$g(z, t) = \frac{\Gamma g_N (N(z, t) - N_0)}{2(1 + \varepsilon P)} \quad (4.10)$$

where  $\Gamma$  is the confinement coefficient of the active layer.  $g_N$  represents the differential gain or differential absorption.  $N_0$  is the carrier density at transparency.  $\varepsilon$  is the gain compression coefficient.  $N$  is the carrier density.  $P$  is the photon density, and  $\delta$  is a detuning factor that accounts for the change of refractive index due to the variation of carrier density.

The time-dependent carrier rate equation in the active layer is written as

$$\frac{dN}{dt} = \frac{J}{qd} - \frac{N}{\tau} - BN^2 - CN^3 - Gv_g P \quad (4.11)$$

where  $J$  is the current injection density,  $q$  is the electron charge,  $d$  is the thickness of the active layer,  $\tau$  is the carrier lifetime,  $B$  and  $C$  are bimolecular and Auger recombination coefficients, respectively,  $G$  is the field gain.

The time-dependent carrier rate equation in the absorber is written as

$$\frac{dN}{dt} = -\frac{N}{\tau} - Gv_g P \quad (4.12)$$

$P$  is the photon density, which is given by the normalized power

$$P = |E^+|^2 + |E^-|^2 \quad (4.13)$$

### 4.3.3 Modeling of Spontaneous Noise

The spontaneous noise  $s_+$  and  $s_-$  are assumed to have a Gaussian distribution that satisfies the correlation

$$\langle s_{\pm}(z, t) s_{\pm}^*(z', t) \rangle = \frac{\beta K R_{sp} \delta(t-t') \delta(z-z')}{v_g} \quad (4.14)$$

$$\langle s_{\pm}(z, t) s_{\pm}(z', t) \rangle = 0$$

where  $R_{sp} = \frac{BN^2}{L}$  is the bimolecular recombination per unit length contributed to spontaneous emission,  $\beta$  is the spontaneous coupling factor, and  $K$  is the transverse Petermann factor.  $\delta(*)$  in this case represents the Delta function.

It has been proved by Petermann [30] that the spontaneous emission fields coupled to the forward and reverse waves have equal amplitudes.

$$s_{\pm}(z, t) = s_+(z, t) = s_-(z, t) \quad (4.15)$$

### 4.3.4 Modeling of Self-phase Modulation

Self-phase modulation (SPM) is caused by changes in the refractive index through carrier density changes. SPM produces variations in the round trip cavity time

and also adds to the excess bandwidth beyond the transform limit. This effect is included in the model through the detuning factor  $\delta$  which can vary along the structure

$$\delta = (\omega_0/c)[n_{eff0} - \Gamma\alpha_m g_N(\lambda_0/4\pi)\Delta N(z, t)] \quad (4.16)$$

where  $c$  is the speed of light at vacuum.  $\Delta N$  is the change of carrier density, and  $\alpha_m$  is the material linewidth enhancement factor.

### 4.3.5 Frequency Dependent Gain Profile

The gain/loss profile in the laser is frequency dependent. This frequency dependent effect is simulated by filtering the optical field gain by a Lorentzian filter. The frequency response for such a filter is

$$H(\omega) = \frac{g(\omega_0)}{[1 + \tau^2(\omega - \omega_0)^2]^{1/2}} \quad (4.17)$$

where  $\omega_0$  is the central frequency,  $\tau$  is a parameter controlling the shape of the filter.

### 4.3.6 Computation Procedure

In order to solve the coupled wave equations 4.8 and 4.9, the finite difference equation approximation is applied to the partial differential terms. For this approach, the laser is divided into a number of equal small sections with length

$$\Delta z = L/M \quad (4.18)$$

where  $L$  is the length of the laser and  $M$  is the number of sections.

The time and spatial steps are taken to be equal to

$$\Delta z = v_g \Delta t \quad (4.19)$$

The Central Difference Method is then used to provide a precise and stable solution. By applying the Central Difference Method to field equations 4.8 and 4.9, we get

$$E^+(z, t + \Delta t) = \frac{1 + \frac{\Delta z}{2}(g - \alpha_s) - i\frac{\Delta z}{2}\delta}{1 - \frac{\Delta z}{2}(g - \alpha_s) + i\frac{\Delta z}{2}\delta} E^+(z - \Delta z, t) + \Delta z s_+ \quad (4.20)$$

$$E^-(z, t + \Delta t) = \frac{1 + \frac{\Delta z}{2}(g - \alpha_s) - i\frac{\Delta z}{2}\delta}{1 - \frac{\Delta z}{2}(g - \alpha_s) + i\frac{\Delta z}{2}\delta} E^-(z - \Delta z, t) + \Delta z s_- \quad (4.21)$$

By choosing  $z = 0$  at the left-hand facet, the boundary condition for the forward and backward waves at the facets can be written as

$$E^+(0, t) = r_L E^-(0, t) \quad (4.22)$$

$$E^-(L, t) = r_R E^+(L, t) \quad (4.23)$$

where  $r_L$  and  $r_R$  are the amplitudes of the facet reflections.

By knowing the field value at time  $t$  and location  $z$ , the fields for forward and backward waves at the next time step  $t + \Delta t$  can be determined at the position  $z + \Delta z$  and  $z - \Delta z$  respectively from Equation 4.20 and Equation 4.21. In each time step, the field gain  $g$ , detuning factor  $\delta$ , effective index  $n_{eff}$  and the carrier density  $N$  will change according to Equation 4.10, 4.16, 4.11 and 4.12.

All equations involved in the calculation are solved numerically. all parameters are assumed to be constant in a subsection. A self-consistency system is formed for the calculation of the electric field  $E^+(z, t)$  and  $E^-(z, t)$  and the carrier density  $N(z, t)$  through the photon density  $P(z, t)$  in each section at each fixed time step  $\Delta t$ .

## 4.4 Device Parameters

The device being simulated is a semiconductor laser with a gain section and a saturable absorber section. The parameters used are shown in Table 4.1

Parameter	Symbol	Value	Unit
Group Velocity	$V_g$	$0.85 \times 10^8$	$ms^{-1}$
Effective Refractive index	$n_{eff}$	3.53	
Internal Cavity Loss	$h$	10	$cm^{-1}$
Width		2	$\mu m$
Depth		0.07	$\mu m$
Confinement Factor	$\Gamma$	0.1	
Wavelength	$\lambda_0$	1550	nm
Injection Current	$I$	80	mA
Carrier Lifetime in Gain Section	$\tau_g$	5.0	ns
Radiation Recombination	$B_g$	$1.5 \times 10^{-10}$	$cm^3 s^{-1}$
Auger Recombination	$C_g$	$1 \times 10^{-29}$	$cm^6 s^{-1}$
Transparency Carrier Density in Gain section	$N_{og}$	$1 \times 10^{18}$	$cm^{-3}$
Output Facet REffectivity	$R$	0.7	
Gain Compression Factor	$\epsilon_g$	$2 \times 10^{-17}$	$cm^3$
Differential Gain	$\alpha_g$	$(0.1 - 2.5) \times 10^{-15}$	$cm^2$
Linewidth Enhancement Factor	$\alpha_H$	2-6	
Carrier Lifetime in Absorber Section	$\tau_a$	5-20	ps
Transparent Carrier Density	$N_{oa}$	$0.75 \times 10^{18}$	$cm^{-3}$
Absorption Compression Factor	$\epsilon_a$	$4 \times 10^{-17}$	$cm^3$
Differential Absorption	$\alpha_a$	$(0.5 - 4) \times 10^{-15}$	$cm^2$
Length of Gain Section		899.193	$\mu m$
Length of Absorber Section		108.694	$\mu m$
Device Length	$L$	1.007887	mm

Table 4.1: Device Parameter for Simulation

A repetition rate around 40GHz is chosen for the simulation primarily because of the trade-off between accuracy of the simulation and the length of simulation time. The spatial step chosen for simulation of this device is  $9.88125 \times 10^{-6}$ . This is equivalent to a time step of  $112fs$  which is much shorter than the carrier lifetime of the device. Thus the dynamic behavior of the laser during

mode-locking can be accurately simulated with this time step. With this time step, the device length has to be relatively short to allow the simulation to finish in a reasonable period of time. It was chosen to be around 1mm which is equivalent to a device with repetition rate of around 40GHz. Note that while choosing the particular value of device lengths and the simulation time step, the spectral characteristic of the laser is taken into consideration. The time step is chosen in such a way that the sampling bandwidth is wide enough to faithfully reproduce the spectrum of the laser while the emission wavelength is located at the center of the modeling bandwidth coinciding with the gain peak of the laser cavity.

## 4.5 Simulation Results on Passive Mode-locking

In this section, the simulation results obtained using the large signal time domain modelling method as presented in the previous section are described.

### 4.5.1 Pulse Repetition Rate under Passive Mode-locking

For the case of passive mode-locking, the repetition rate of the pulse train is determined by the round trip time. For the device being modeled, the repetition rate is given by

$$rep = \frac{V_g}{2 \times 1.007887 \times 10^{-3}} = 42.167HGz \quad (4.24)$$

A typical pulse train is shown in Figure 4.1. As can be observed from the figure, the repetition rate is indeed close to 42.167GHz.

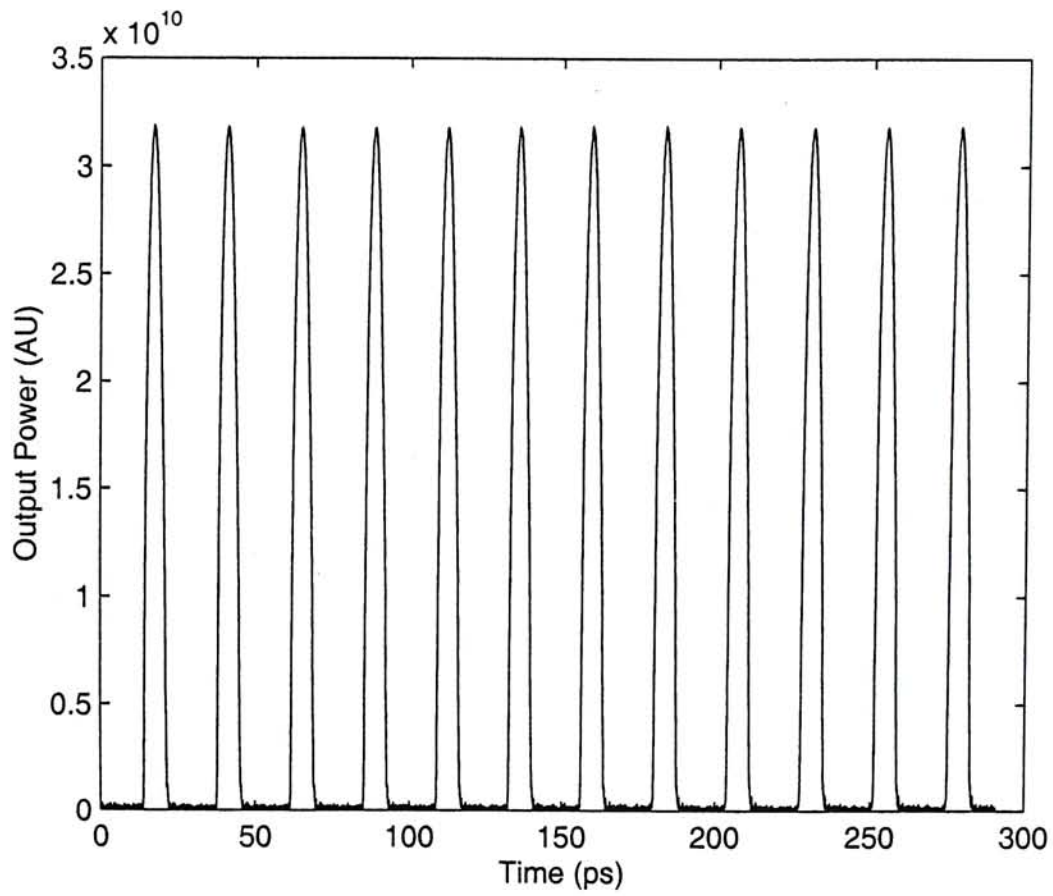


Figure 4.1: A typical mode locked pulse trains

### 4.5.2 The effect of Differential Gain and Differential Absorption on Mode-locking Regimes

In this section, the effect of different combinations of differential gain and differential absorption parameters on the passive mode-locking regimes are studied. With the absorber carrier lifetime fixed at  $5ps$ , the differential gain and differential absorption parameters are varied over a wide range. The simulation result is shown in Figure 4.2.

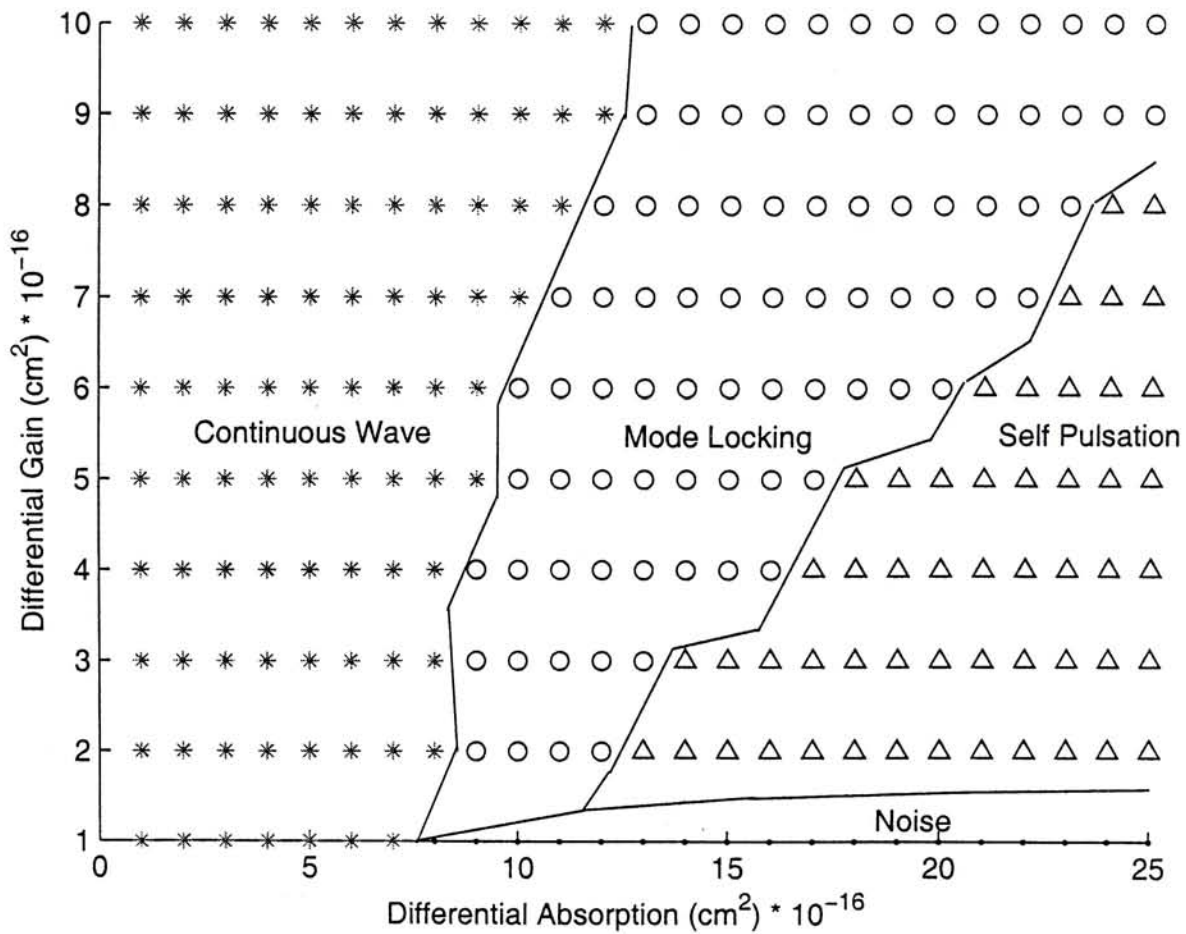


Figure 4.2: Different regimes of mode locking operation

These results indicates a number of operation regimes, namely mode locking, continuous wave, self-pulsation [31] and noise output [32], for passive mode

locking laser. The waveform of these outputs are shown in Figure 4.3

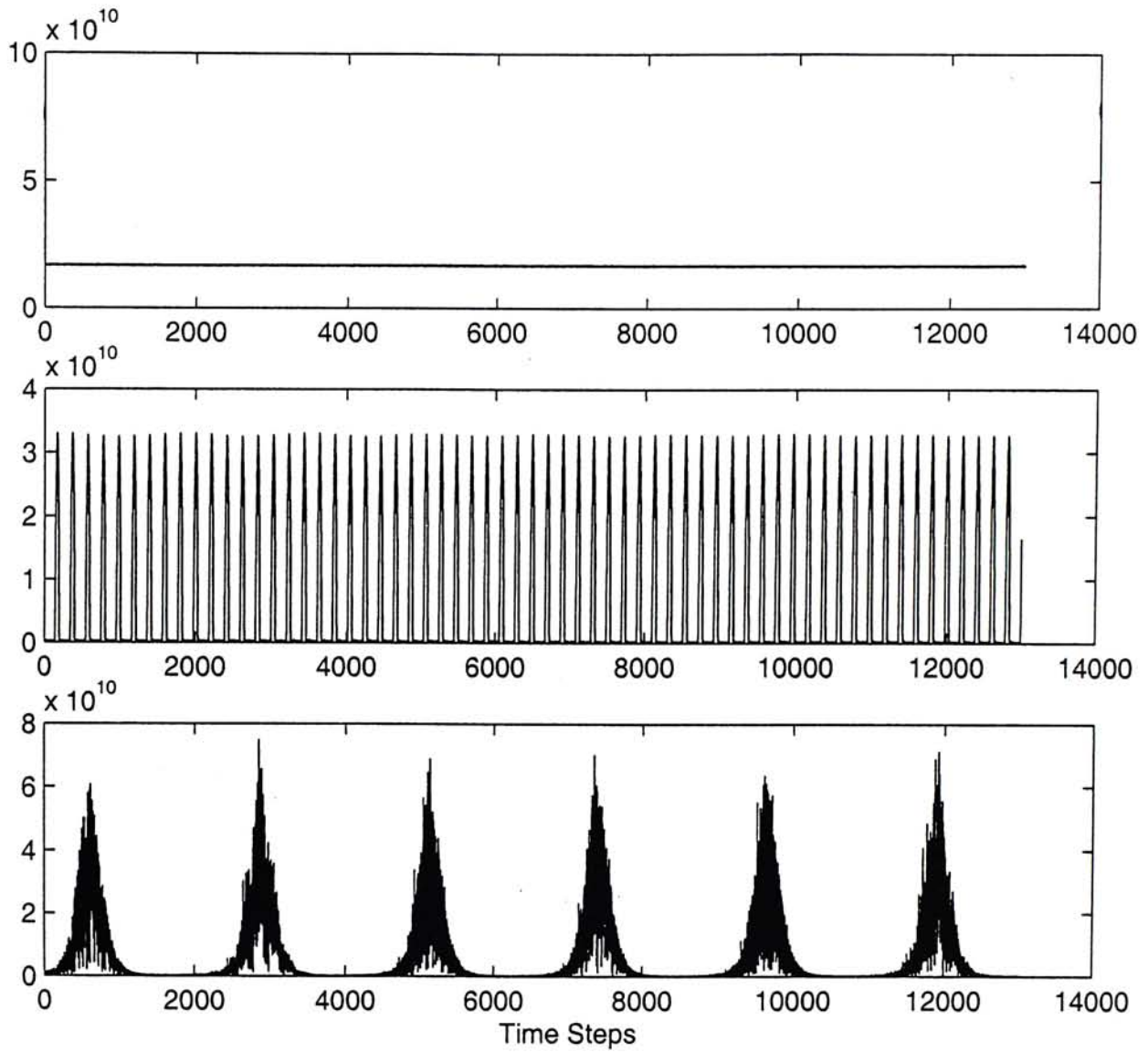


Figure 4.3: The output of mode-locked laser in CW, mode-locked and self-pulsation regimes

The region in which mode locking occurs agrees with the well-known necessary conditions for mode-locking in semiconductor lasers

$$\tau_a < \tau_g \quad (4.25)$$

$$\alpha_a > \alpha_g \quad (4.26)$$

That is, the absorber carrier lifetime  $\tau_a$  needs to be smaller than gain carrier lifetime  $\tau_g$  and the differential absorption  $\alpha_g$  has to be larger than the differential gain  $\alpha_g$  [4]. It can also be observed that the lower bound and the upper bound of the passive mode locking range tend to shift as  $\alpha_g$  increases giving a wider operating range for passive mode locking.

As  $\tau_a$  increases, passive mode locking will give way to self-pulsation. This can be explained by using the time dependent carrier rate equation in the absorber section

$$\frac{dN}{dt} = -\frac{N}{\tau_a} - \frac{\Gamma\alpha_a(N - N_0)}{1 + \varepsilon P}v_gP \quad (4.27)$$

Using this equation, the steady state carrier concentration can be expressed as

$$N = \left(\frac{N_0}{1 + \varepsilon P}v_gP\right) / \left(\frac{1}{\Gamma\alpha_a\tau_a} + \frac{1}{1 + \varepsilon P}v_gP\right) \quad (4.28)$$

Increasing the differential absorption has the effect of decreasing the rate of change of the absorber carrier concentration and increasing the absorber carrier concentration. Initially, large differential absorption would prevent the laser from lasing. The carrier concentration and gain in the cavity would then build up with time until the threshold is reached. A large optical pulse bleaches the absorber but then depletes the carrier density so that any gain is quenched and pulse production ceases. This process continues repeatedly thus self-pulsation can be observed.

### 4.5.3 The Effects of Linewidth Enhancement Factor and Absorber Carrier Lifetime on Mode-locking Pulse Width

To observe the effect of the absorber carrier lifetime and the linewidth enhancement factor on the pulse width, the pulsewidth of the generated pulses are recorded for a range of different values of linewidth enhancement factor and absorber carrier lifetime. It is found that changing linewidth enhancement factor and the absorber carrier lifetime will change the pulse width as shown in Figure 4.4.

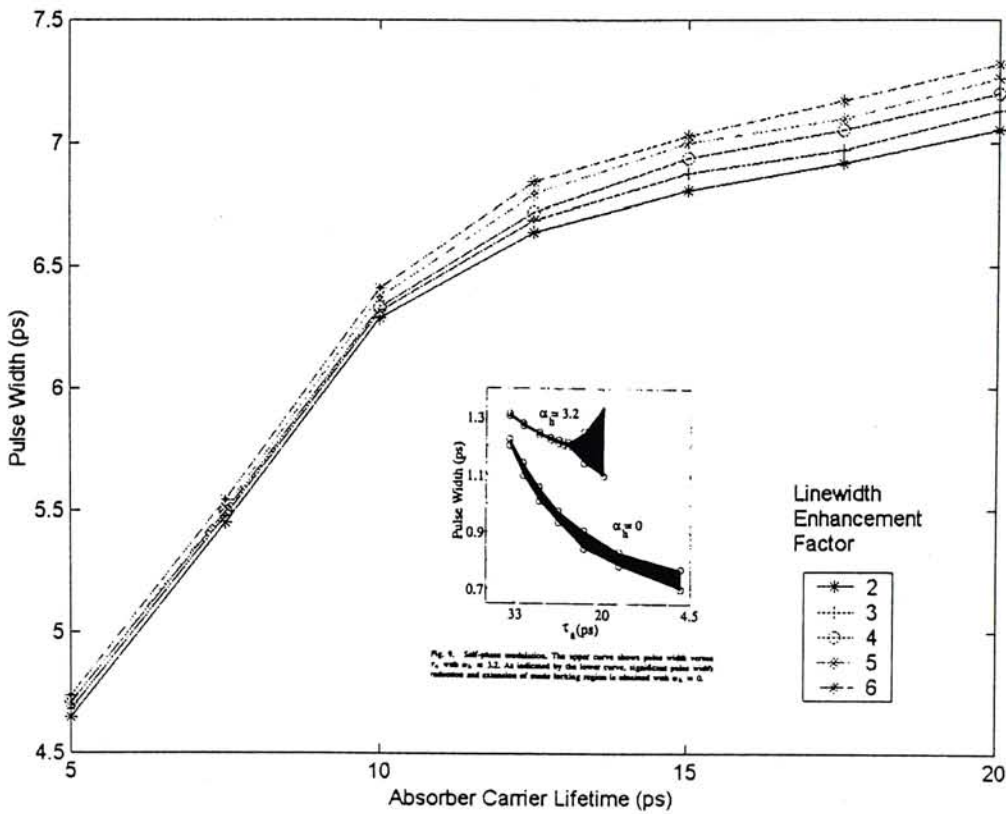


Figure 4.4: Pulse width vs line width enhancement factor at different absorber carrier lifetime

It can be seen from Figure 4.27 that decreasing absorber carrier lifetime will result in the increase of the rate of change of absorber carrier concentration. The higher rate of change would allow the absorber to have a higher absorption rate, thus it is reasonable to observe that a shorter absorber carrier lifetime would give rise to a pulse train with narrower pulse width as shown in the figure. This result also generally agrees with the simulation result in [33] as shown in the inset of Figure 4.4. Note that the inset is in linear-log scale. Increasing linewidth enhancement factor can also increase the pulse width. However, its effect is only minimal when compared with that of absorber carrier lifetime.

## **4.6 Simulation Results on Hybrid and Subharmonic Mode-locking**

Besides passive mode locking, the model derived in this chapter can also be used to simulate the behavior of hybrid and subharmonic mode locking. In this section, the simulation results are presented.

### **4.6.1 Modeling the Effect of Modulation on Absorber Section**

To modulate the reverse bias voltage of the absorber section, a sinusoidal electrical signal is applied to the reverse bias together with a DC biasing offset at the saturable absorber. To simplify the simulation, it is assumed that the external signal would only modulate the absorber carrier lifetime [25]. Hence the effect

can be simulated by replacing the constant value  $\tau_a$  by

$$\tau_a = \tau_{dc} + \tau_{ac} \sin\left(2\pi \frac{f}{N_s} t\right) \quad (4.29)$$

where  $N_s$  is the subharmonic number and  $f$  represents the fundamental modulation frequency, which is equal to inverse of round-trip travelling time of the laser cavity.

### 4.6.2 Modulation Phase Change Dynamics

The RF signal applied to the SA section of the mode-locked laser serves as a reference to which the output optical pulses is synchronized. If the phase of the RF signal is changed, the relative position of the output pulses will inevitably be changed. This has been experimentally demonstrated and reported in [34]. However, the detail phase change dynamics has not yet been studied primarily because such phenomenon is very difficult to observe experimentally. In this section, the dynamic behavior of the mode locked laser during phase tuning is studied using the simulation model.

As confirmed by the experimental demonstration, the mode-locked optical pulses would appear in different relative positions as the phase of the RF driving signal changes. The amount of shift of the pulses is proportional to the amount of phase change in RF driving signal as can be observed in Figure 4.5.

This change, however, does not occur instantly when the RF phase is changed. The laser would undergo a transient period before the optical pulses finally stabilized into the new steady state position. The duration of the transient period is found to be related to 2 factors, the amount of phase shift and the applied RF power. Their effects are summarized in Figure 4.6. Here, we found that

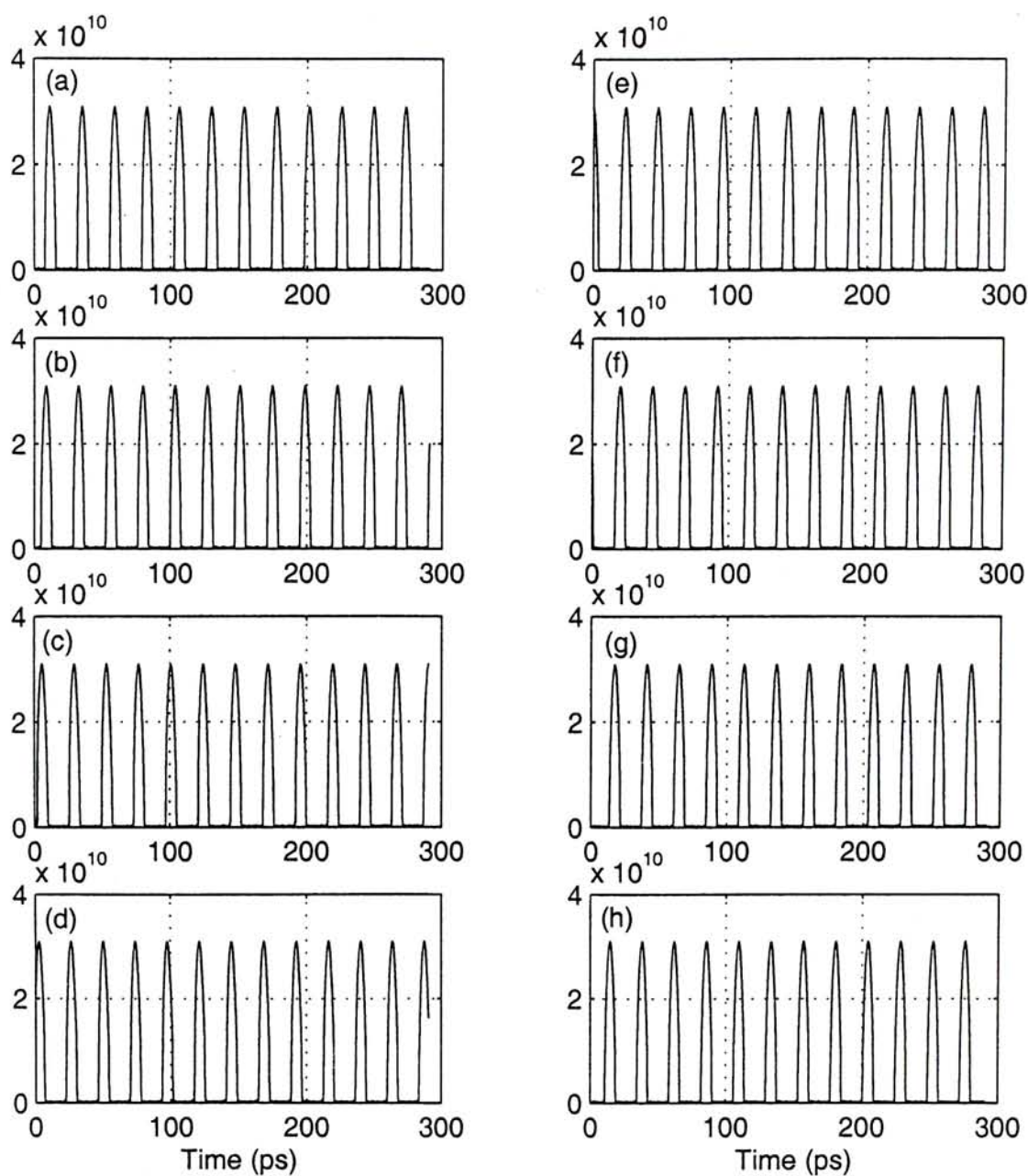


Figure 4.5: Relative position of the pulses when the phase of the RF is changed for an amount of from 0 (a) to  $\frac{7\pi}{4}$  (h)

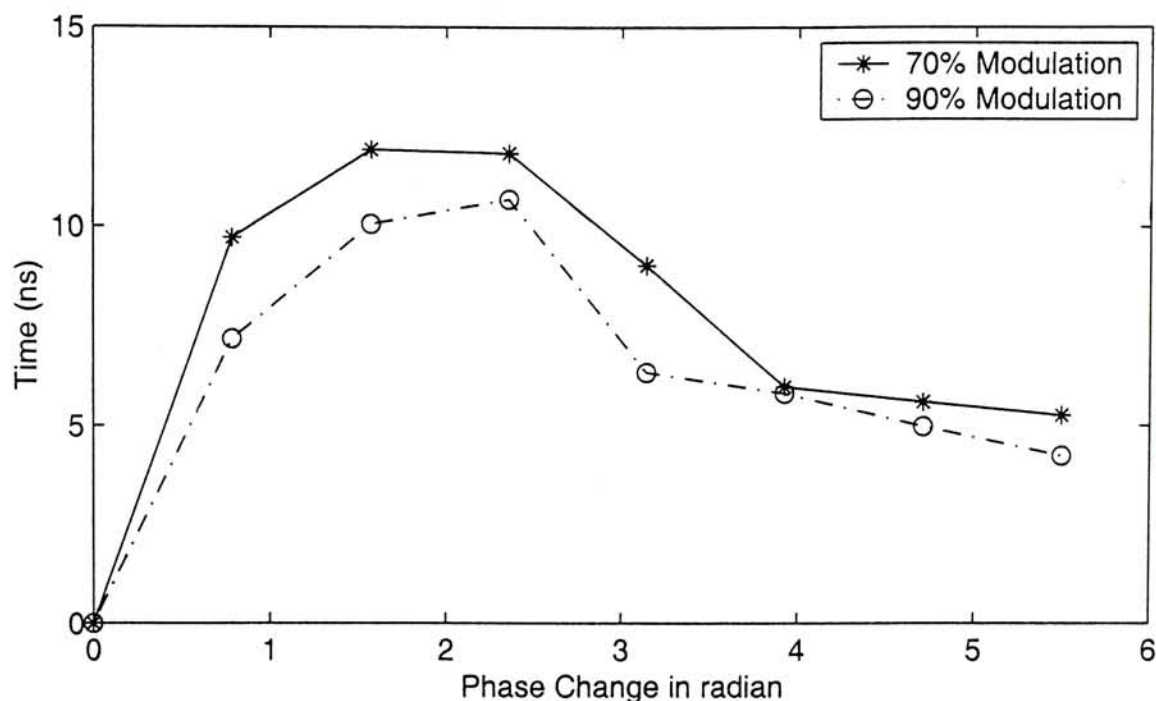


Figure 4.6: Transient time for laser output due to RF phase tuning

the absolute amount of phase change plays an important role in deciding the transient duration. Since a change of  $7\pi/4$  in RF phase is equivalent to shifting the RF phase backward by the amount of  $\pi/4$ , the maximum amount of phase change that could occur is actually  $\pi$ . The maximum amount of transient duration occurs at about  $\frac{3\pi}{4}$  as can be seen in Figure 4.6. A further study is needed on this phenomenon. The amount of RF power applied to the laser also affects the transient duration. This effect can also be found in the figure where the curve using 70% modulation appears above the one using 90% modulation, which simulates a higher input RF power. This is reasonable as the higher the RF signal power the deeper the modulation on the carrier lifetime of the saturable absorber would be. This helps to bring the pulses to the new position in a shorter time.

During this transient period, the amplitude and the width of the pulses

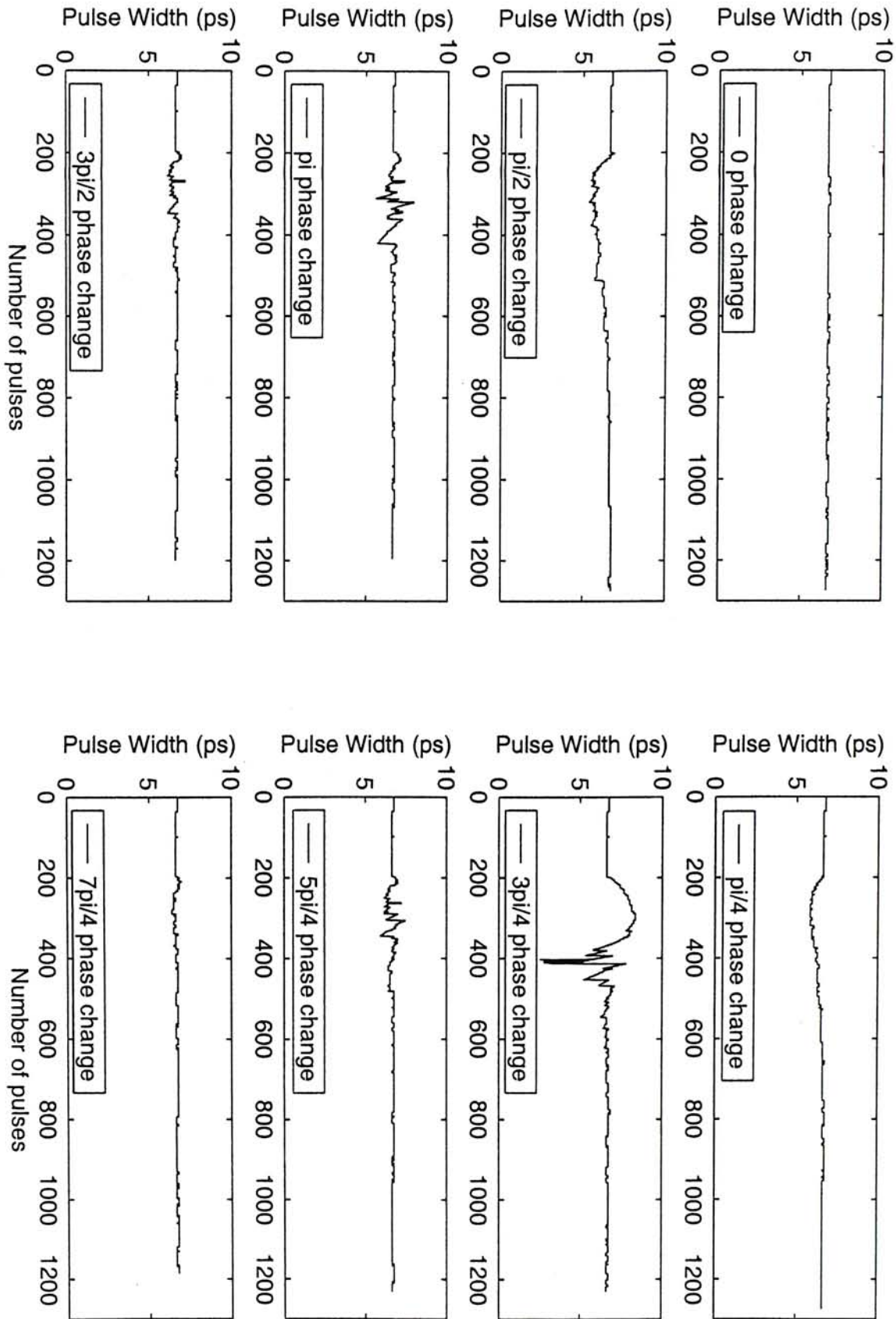


Figure 4.7: The change of pulse width during phase tuning with 70% modulation of RF modulation

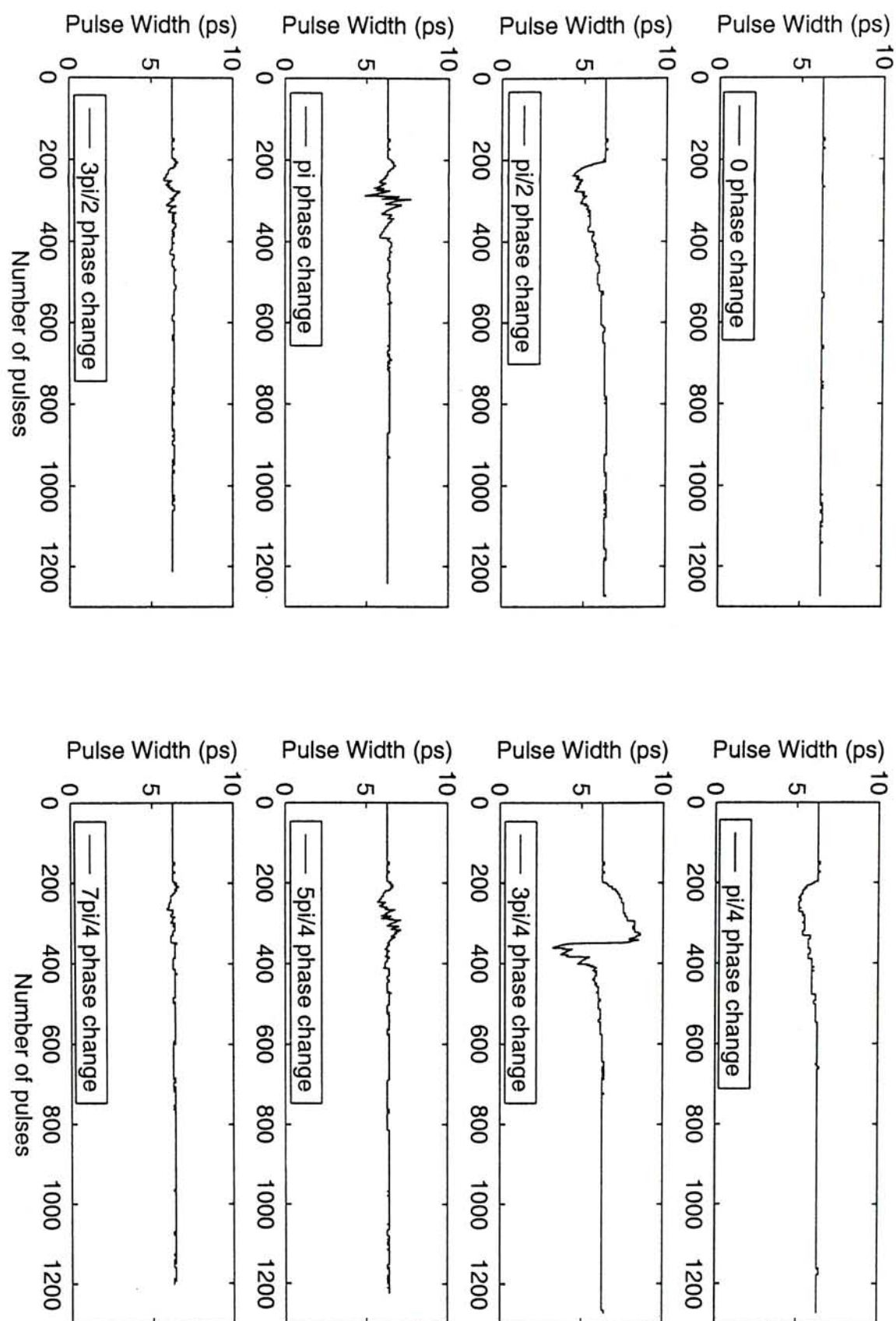


Figure 4.8: The change of pulse width during phase tuning with 90% modulation of RF modulation

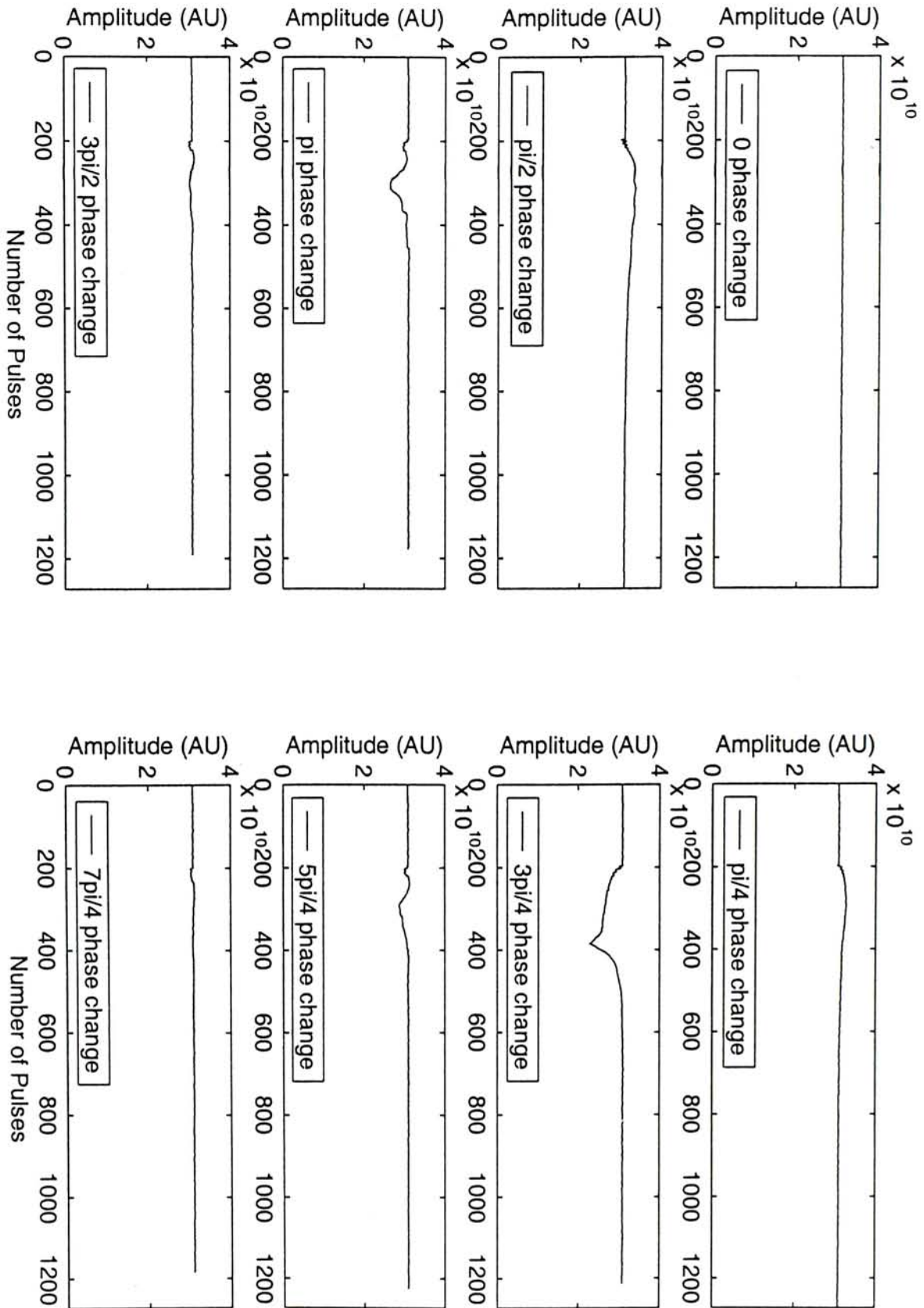


Figure 4.9: The change of pulse amplitude during phase tuning with 70% modulation of RF modulation

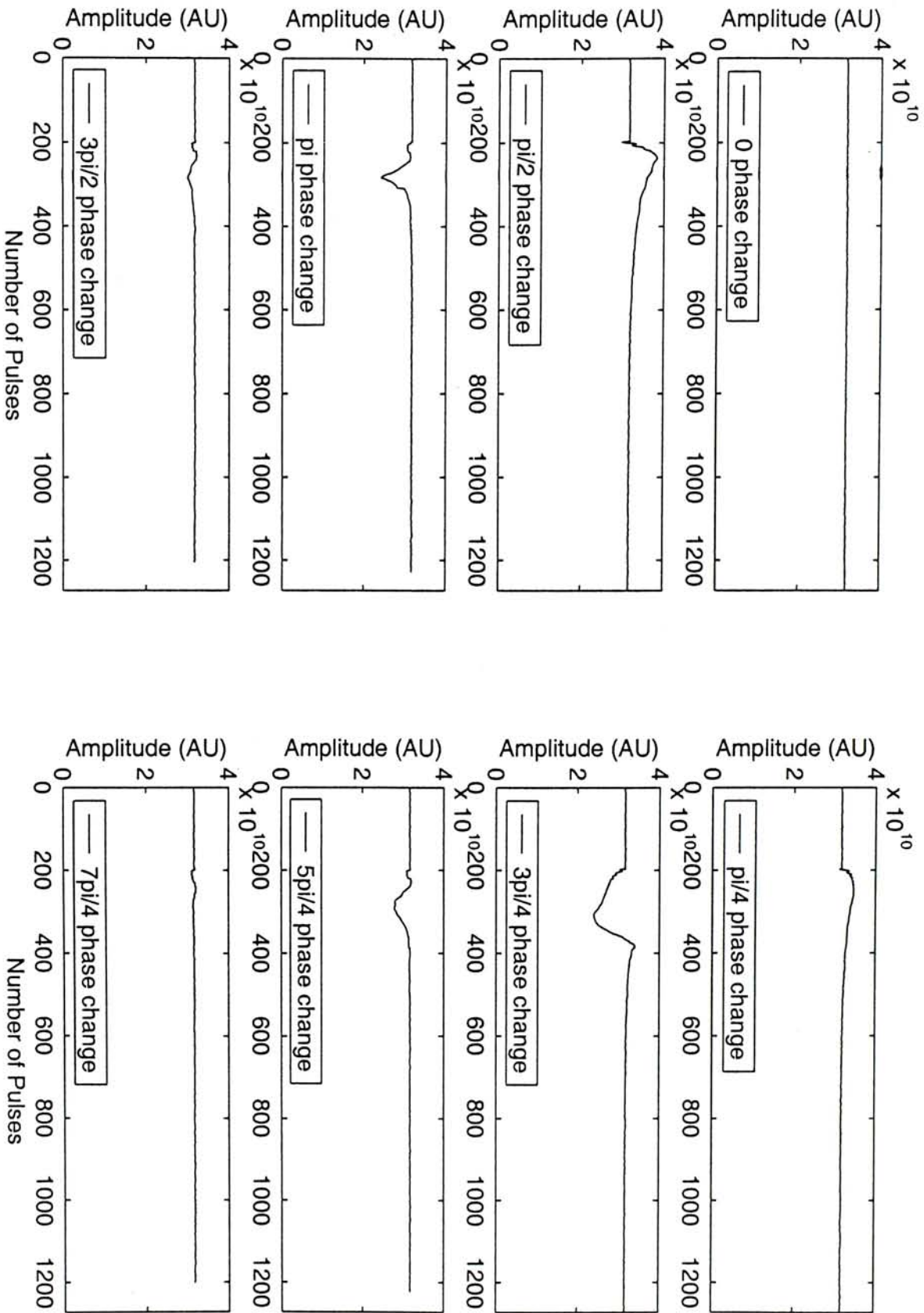


Figure 4.10: The change of pulse amplitude during phase tuning with 90% modulation of RF modulation

change with time. The dynamic variation of amplitude and pulse width shows high dependence on the amount of phase change on the RF signal, as can be observed in Figure 4.7, 4.8, 4.9 and 4.10 respectively.

### **4.6.3 Subharmonic Mode-Locking Induced Amplitude Modulation**

For a high repetition rate hybrid mode-locked laser operating at 40GHz or above, it is difficult to find an RF signal source that operates at that high frequency. In this case, subharmonic hybrid mode locking can be utilized. The subharmonic mode locking method make use of an RF signal at a frequency that is one of the subharmonics of the fundamental frequency. The drawback, as reported in [35], is that the subharmonic RF signal would cause amplitude modulation to be imposed on the output pulse train. Amplitude modulation on the pulse train would cause higher bit error rate in communication systems and would degrade the performance of the whole system. The phenomenon of amplitude modulation is investigated in this part.

The effect of subharmonic RF driving signal on the amplitude of the pulse train is shown in Figure 4.11. It can be clearly seen that amplitude modulation is indeed present in the output pulse train.

To quantitatively measure the effect of amplitude modulation, a measurement parameter has to be chosen in such a way that larger amplitude modulation would give rise to a larger value of that parameter. We define this parameter as the ratio of the standard deviation  $\sigma$  of the output pulse amplitude modulation

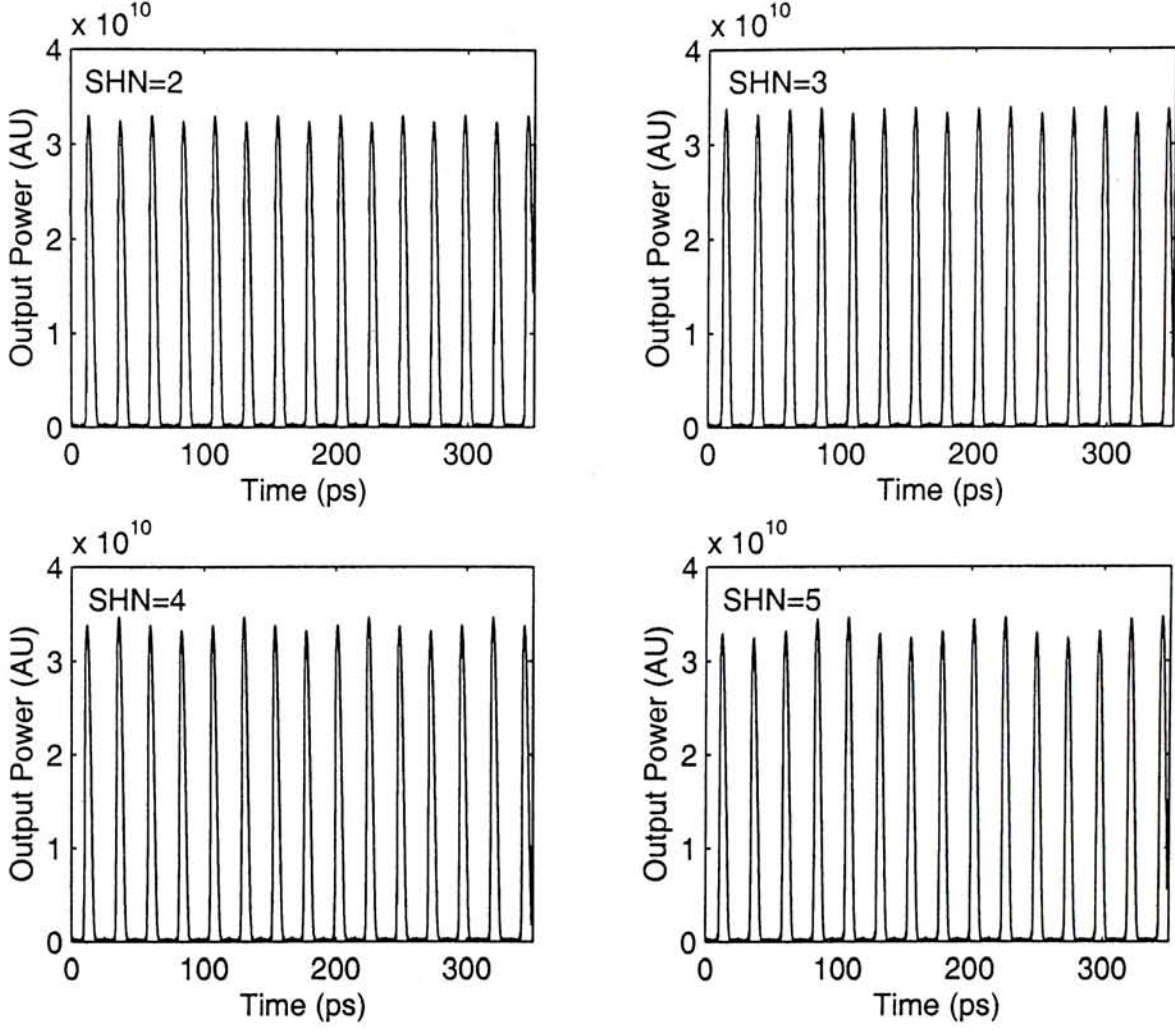


Figure 4.11: Pulse train for subharmonic number 2, 3 4 and 5 respectively

and the mean  $\mu$  of the output pulse amplitude. That is

$$\text{AmplitudeModulationParameter} = \frac{\sigma}{\mu} \quad (4.30)$$

The subharmonic number dependence of the amplitude modulation parameter is presented in Figure 4.12. For a constant RF power, the degree of amplitude modulation would increase as the subharmonic number increases. A possible explanation, as suggested in [35], is that at a smaller subharmonic number, the driving frequency is actually higher. This frequency falls outside the modulation frequency band of the laser device and the laser cannot respond fast enough for

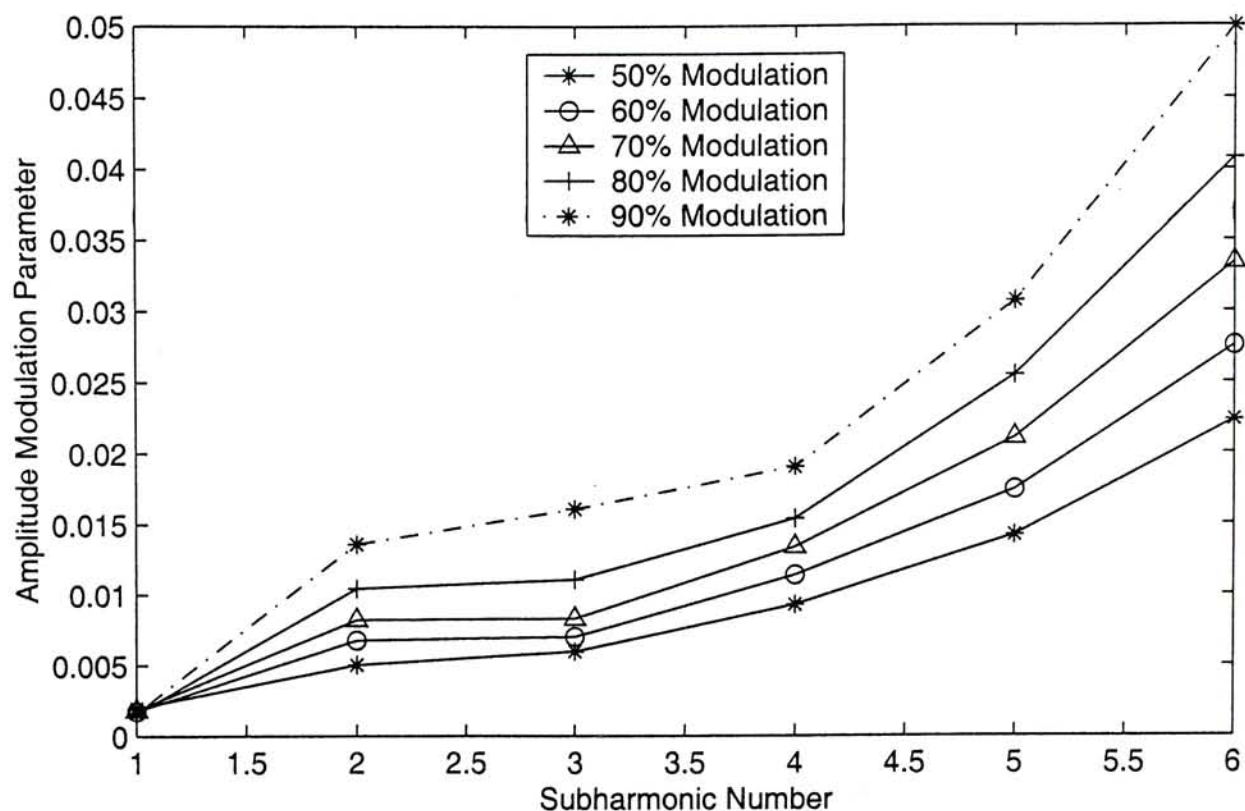


Figure 4.12: Amplitude modulation parameter vs Subharmonic Number

this modulation signal. Thus for subharmonic mode locking, it is preferable to use an RF signal with a smaller subharmonic number.

Another trend that can be observed from Figure 4.12 is that as the RF input power is increased, which results in the increase of modulation depth, the amplitude modulation increases as well.

## 4.7 Summary

In this chapter, a numerical model is derived from time dependent coupled wave equations to simulate the dynamics of passive and hybrid mode-locking. Using this model, a number of phenomena for mode-locked laser diode are investigated. These include the differential gain and differential absorption dependence of

mode locking regimes, output pulse width dependence on the absorber carrier lifetime and linewidth enhancement factor and the amplitude modulation for subharmonic mode-locking. The RF phase change dynamics in the mode-locking laser has also been investigated for the first time.

# Chapter 5

## Conclusion

### 5.1 Summary of the Thesis

The objective of this thesis is to explore the feasibility of utilizing semiconductor mode-locked laser sources in a fast channel tunable transmitter and to investigate the behavior of a mode-locked laser diode through numerical simulation.

Chapter 2 presented an overview of all-optical time division multi-access networks. The network architectures including broadcast network and switch-based network were described. The enabling technologies for OTDMA networks, such as ultrafast pulse source, multiplexer, demultiplexer, clock recovery circuit, were also presented. In chapter 3 an experimental demonstration of channel tunable transmitter for OTDM network using Mode-locked laser diode was reported. The transmitter operates in a 40-Gb/s OTDM network with per-channel data rate of 10 Gb/s. The channel tuning time for this device is about 2 ns. This value was compared with the tuning time of gain-switched laser and fiber ring laser. It was found that the tuning time for a gain-switched FP laser may be

shorter than that of mode-locked diode laser while the fiber ring laser has the longest tuning time, primarily due to the long cavity length.

In Chapter 4, a numerical model for mode-locked laser was derived from well-known time dependent coupled wave equations. This model was used to simulate the behavior of passive and hybrid mode-locked diode laser. A number of parameters were changed to observe the effects on laser output. The dependence of mode-locked regimes on differential gain and differential absorption parameters was investigated. It was found to match the theoretical mode locking conditions. Pulse width of mode-locked laser was found to be related to the absorber carrier lifetime as well as the linewidth enhancement factor. For hybrid mode-locking, we, for the first time, investigated the dynamics of the laser when the phase of the RF signal is shifted. The transient time was found to related to the amount of phase shift as well as the input RF power. During this transient period, the pulse width as well as the pulse amplitude would undergo a series of fluctuation before settling down to a steady state. RF driving signal induced amplitude modulation on subharmonic mode-locked laser was also investigated in the chapter. Our simulation suggests that lower subharmonic number would induce less amplitude modulation.

## **5.2 Future Work**

Due to the device availability problem, a fully functional tunable transmitter node for OTDM network using the scheme proposed in this thesis was not implemented. For future work, a network node incorporating pulse generation, channel selection and data modulation can be constructed. Another interesting

continuation on current project would be to use the mode-locked laser device to construct a network node that performs simultaneous wavelength conversion, synchronization and data regeneration by using injection locking properties of mode-locked diode lasers.

For the numerical simulation, the modelling method can be further improved to accept external optical input and simulate the dynamics of optical injection locking. Recently, mode-locked lasers with a DBR section has been implemented [36]. By applying different voltage to this DBR section, the pulse repetition rate of the laser can be slightly tuned. The effect of a DBR section on the mode-locking process can be investigated using the numerical model described in this thesis, with some modifications.

# Bibliography

- [1] D. J. G. Mestdagh. *Fundamentals of Multiaccess Optical Fiber Networks*. Artech House, 1995.
- [2] S. Nogiwa, Y. Kawaguchi, H. Ohta, and Y. Endo. Generation of gain-switched optical pulses with very low timing jitter by using external cw-light injection seeding. *Electron. Lett.*, 36:235–236, 2000.
- [3] P.P. Vasil'ev, I. H. White, and M. J. fice. Narrow line high power picosecond pulse generation in a multicontact distributed feedback laser using modified q switching. *Electron. Lett.*, 29(6):561–563, 1993.
- [4] H.A. Haus. Theory of mode locking with a slow saturable absorber. *IEEE J. Quantum Electron.*, QE-11(9):736–746, 1975.
- [5] L.M. Zhang, S.F. Yu, M.C. Nowell, D.D. Marcenac, J.E. Carroll, and R.G.S. Plumb. Dynamic analysis of radiation and side-mode suppression in a second-order dfb laser using time-domain large signal traveling wave model. *IEEE J. Quantum Electron.*, 31:1389–1395, 1994.

- [6] V.W.S. Chan, K.L. Hall, E.Modiano, and K.A. Rauschenbach. Architectures and technologies for high-speed optical data networks. *J. Lightwave Technol.*, 15:2146, 1998.
- [7] R.A. Barry et al. All-optical network consortium– ultrafast tdm networks. *J Lightwave Technol./IEEE J. Select. Areas Commun.*, 14:999, 1996.
- [8] P. Gunning, J.K. Lucek, D.G. Moodie, K. Smith, D. Pitcher, Q. Badat, and A.S Siddiqui. Synchrolan: 40git/s optical-tdma lan using installed blown-fibre. *Electron. Lett.*, 34(5):488–490, 1998.
- [9] Chun-Kit Chan, Lian-Kuan Chen, F. Tong, and K.W. Cheung. Realization of a time-slot access wdma dual bus/ring packet network node using centralized light sources. *IEEE Photon. Technol. Lett.*, 9:1661 –1663, 1997.
- [10] N. F. Maxemchuk. The manhattan street network. In *Proc. IEEE GLOBE-COM '85*, pages 255–261, 1985.
- [11] Yu B.Y., Glesk I., and Prucnal P.R. Analysis of a dual-receiver node with high fault tolerance for ultrafast otdm packet-switched shuffle networks. *J. Lightwave Technol.*, 16:736–744, 1998.
- [12] K. Zoiros, K. Vlachos, T. Stathopoulos, C. Bintjas, and H. Avramopoulos. 40 ghz mode-locked soa fiber ring laser with 20 nm tuning range. In *Proc. OFC'2000*, pages ThR3–1, 2000.
- [13] Peter Vasil'ev. *Ultrafast Diode lasers: Fundamentals and Applications*. Artech House Publishers, London, 1995.

- [14] K. Y. Lau. Gain-switching of semiconductor injection lasers. *Appl. Phys. Lett.*, 52(4):257–259, 1988.
- [15] Kung-Li Deng, Koo Il Kang, I. Glask, and P Prucnal. A 1024-channel fast tunable delay line for ultrafast all-optical tdm networks. *IEEE Photon. Technol. Lett.*, 9:1496–1498, 1997.
- [16] S. Kawanishi, H. Takara, K. Uchiyama, T. Kitoh, and M. Saruwatari. 100 gbit/s, 50 km, and nonrepeated optical transmission employing all-optical multi/demultiplexing and pll timing extraction. *Electron. Lett.*, 29(12):1075–1077, 1993.
- [17] J.P. Sokoloff, P.R. Prucnal, I. Glesk, and M. Kane. A terahertz optical asymmetric demultiplexer (toad). *IEEE Photon. Technol. Lett.*, 57:787–790, 1993.
- [18] K.L. Hall and B.S. Robinson. Bit error rate characterization of 100 gb/s all-optical demultiplexers. In *CLEO '99*, pages 214 –215, 1999.
- [19] S. Kawanishi, H. Takara, T. Morioka, O. Kamatani, K. Takiguchi, T. Kitoh, and M. Saruwatari. 400 gbit/s tdm transmissio of 0.98ps pulses over 40km employing dispersion slope compensation. In *OFC'96*, page PD24, 1996.
- [20] H. Yokoyama, Y. Hashimoto, H. Kurita, and I. Ogura. All-optical subharmonic clock recovery and demultiplexing. In *Proc. OFC'2000*, 2000.
- [21] N.S. Patel, K.A. Rauschenbach, and K.L. Hall. 40-gb/s demultiplexing using an ultrafast nonlinear interferometer (uni). *IEEE Photon. Technol. Lett.*, 8(12):1695–1697, 1996.

- [22] Chun-Kit Chan, Lian-Kuan Chen, and Kwok-Wai Cheung. A fast channel-tunable optical transmitter for ultrahigh-speed all-optical time-division multiaccess. *IEEE J. Select. Area Commun.*, 14(5):1052–1056, 1996.
- [23] I. Shake, H. Takara, S. Kawanishi, and M Saruwatari. High-repetition-rate optical pulse generation by using chirped optical pulses. *Electron. Lett.*, 34(8):792–793, 1998.
- [24] H. Kurita, I. Ogura, and H Yokoyama. *IEICE Trans. Electron.*, E81-C:129–139, 1998.
- [25] E.A. Avrutin, J.M. Arnold, and J.H. Marsh. Analysis of dynamics of monolithic passively mode-locked laser diodes under external periodic excitation. *IEEE Proc. Optoelec.*, 143:81–88, 1996.
- [26] P.T. Ho, L.A. Glasser, E.P. Ippen, , and H.A. Haus. Mode-locking of semiconductor laser. *Appl. Phys. Lett.*, 33:241–243, 1978.
- [27] Y.K. Chen and M.C. Wu. Monolithic colliding pulse mode-locked quantum-well lasers. *IEEE J. Quantum Electron.*, 28:2176–2185, 1992.
- [28] K.Y. Lau. Narrow-band modulation of semiconductor lasers at millimeter wave frequencies ( $>100\text{ghz}$ ) by mode locking. *IEEE J. Quantum Electron.*, 26:250–261, 1990.
- [29] Govind P. Agrawal. *Fiber-Optic Communication Systems*. John Wiley and Sons PTE LTD., 1st edition, 1993.
- [30] John Carroll, James Whiteaway, and Dick Plumb. *Distributed feedback semiconductor lasers*. SPIE Optical Engineering Press, 1998.

- [31] J.Palaski and K.Y. Lau. Parameter ranges for ultrahigh frequency mode locking of semiconductor lasers. *Appl. Phys. Lett.*, 59:7–9, 1991.
- [32] A.E. Siegman. *Lasers*. University Science Books, 1986.
- [33] D.J. Jones, L.M. Zhang, J.E. Carroll, and D.D. Marcenac. Dynamics of monolithic passively mode-locked semiconductor lasers. *IEEE J. Quantum Electron.*, 31(6):1051–1058, 1995.
- [34] W. Hung, L.K. Chen, F. Tong, K.-P. Ho, L.Y. Chan, Shimizu T., and Yokoyama H. Demonstration of a 10 gb/s channel-tunable mode-locked laser transmitter for otdm networks. In *Proc. LEOS '99*, volume 2, pages 539–540, 1999.
- [35] T. Hoshida, H.F. Liu, M. Tsuchiya, Y. Ogawa, and T. Kamiya. Extremely low-amplitude modulation in a subharmonically hybrid mode-locked monolithic semiconductor laser. *IEEE Photon. Technol. Lett.*, 8(9):1160–1162, 1996.
- [36] A. Nirmalathas, H.F. Liu, Z. Ahmed, D. Novak, and Y. Ogawa. Subharmonic synchronous and hybrid mode-locking of a monolithic dbr laser operating at millimeter-wave frequencies. *IEEE Photon. Technol. Lett.*, 9:434–436, 1997.



CUHK Libraries



003803449